On computation of oscillating integrals of ship-wave theory

Oleg V. Motygin

Institute of Problems in Mechanical Engineering, Russian Academy of Sciences, V.O., Bol'shoy pr., 61, 199178 St. Petersburg, Russia
e-mail: o.v.motygin@gmail.com

arXiv:1411.0321v1 [math.NA] 2 Nov 2014

Abstract

Green's function of the problem describing steady forward motion of bodies in an open ocean in the framework of the linear surface wave theory (the function is often referred to as Kelvin's wave source potential) is considered. Methods for numerical evaluation of the so-called 'single integral' (or, in other words, 'wavelike') term, dominating in the representation of Green's function in the far field, are developed. The difficulty in the numerical evaluation is due to integration over infinite interval of the function containing two differently oscillating factors and the presence of stationary points. This work suggests two methods to approximate the integral and its derivatives. First of the methods is based on the idea suggested by D. Levin in 1982 — evaluation of the integral is converted to finding a particular slowly oscillating solution of an ordinary differential equation. To overcome well-known numerical instability of Levin's collocation method, an alternative type of collocation is used; it is based on a barycentric Lagrange interpolation with a clustered set of nodes. The second method for evaluation of the wavelike term involves application of the steepest descent method and Clenshaw–Curtis quadrature. The methods are numerically tested and compared for a wide variety of parameters.

Keywords:
Ship waves, Kelvin wave source, Green's function, Oscillatory integral, Levin method, Clenshaw–Curtis quadrature, Barycentric Lagrange interpolation, Chebyshev points
2000 MSC: 65D30, 65D05, 34B27, 76B07, 76B20

1 Introduction

The steady motion of a ship in calm water is a classic problem of hydrodynamics, significant for engineering and ship design because of its applicability to prediction of wave pattern and wave resistance. As early as in 1887, Lord Kelvin [55] first provided a mathematical description of the wave pattern created by an object moving forward with a constant speed; the familiar V-shaped pattern behind a ship (still being in study, see e.g. [52, 51, 9] and references therein) now bears his name. Starting from Lord Kelvin's work, substantial efforts have been spent to investigation of the ship wave problem and determining the wave resistance. At this, an extensive literature has been produced; comprehensive reviews can be found, e.g. in [63, 62, 40, 12, 32, 31]. In particular, much attention has been paid to potential models and linearized statements similar to that considered in the present work.

An important role in the linear theory of ship waves and wave resistance is played by the Kelvin wave source potential, which may also be identified as the Green's function of the Neumann–Kelvin problem. This potential describes a source moving with a constant horizontal velocity in an ideal incompressible fluid having a free surface; fluid's motion is irrotational and steady-state in a coordinate system attached to the source. The Kelvin wave source potential is fundamental in the theory and applications — for instance, a solution of the problem of the flow past a moving ship is often sought as a distribution of the sources on ship's hull. Considerable efforts in the analysis of the Green's function has resulted in a vast literature (see [31] and references therein) with special interest to the far field behaviour of the source (see e.g. [12, 39]) and to development of efficient and accurate algorithms for computing Kelvin's potential.

A number of representations of the Green's function have been derived (see [44]). Generally, the Green's function is divided into three terms: the singular (Rankine) one, whose computation is elementary; the wavelike (referred to as 'single integral') term — oscillating and dominating in the far field; the near-field nonoscillatory term (for historical reasons often referred to as 'double integral term'). Detailed mathematical analysis of the behavior of the near-field and the far-field terms can be found in [13, 39, 31]. It is known that the 'double integral term' can be expressed as a single integral, in particular, a number of such representations in terms of the exponential integral function can be found in [54, 44]. This allows realization of fast and effective schemes for numerical evaluation of the 'double integral term'. A practical numerical implementation can be found in [42]; further development for the efficacy and accuracy in computation of the near-field term is described in [50].

At the same time, the question of evaluation of the wavelike term is only partly solved. The main difficulty in computation of the term is due to the presence of two oscillating factors of different nature in the integrand, which can have stationary points, and the infinite interval of integration. Besides, there is a difficult limiting case: it was shown in [58] (more details are given in [13, 59]) that the track of the source moving in the free surface is a line of essential singularities. Near the line the wave elevation oscillates with indefinitely increasing amplitude and indefinitely decreasing wavelength. (It is interesting that introducing of surface tension in the formulation of the problem is reported in [6] to eliminate the singularity of the Green's function.)

Most of the existing methods for evaluation of the wavelike term are based or involve two very useful expansions given in [5]: convergent series and an asymptotic one (completed in [58]). However, the summation of such series is not a trivial computational task, it leads to poor accuracy when the source and the field points are close to the free-surface, the method is vulnerable to severe numerical problems because of the presence of very large in magnitude alternating terms and the criteria to choose one of the expansions is difficult to determine. Details of numerical algorithms using the expansions, discussion of their applicability and heuristic criteria of choice between the algorithms can be found in [2, 3, 38, 50]. Another approach in [61] to calculation of the wavelike term is also based on the Green's function representation [5] but the work is in terms of integrals as opposed to the use of the series. Computation of the wavelike term near the track was discussed in [7] where expansions of the function and numerical algorithms are given.

In the present work our purpose is to elaborate alternative, accurate and fast computation methods to approximate the wavelike term. Our consideration is based on recently developed techniques for evaluation of integrals of oscillating functions. The quadrature of oscillating integrals is a very important computational problem (widely considered as a difficult one) appearing in a wide range of applications. The field has enjoyed a recent upsurge of interest and substantive developments with a number of old methods being enhanced and new ones being suggested. Amidst them we mention the numerical steepest descent (see [26, 10]), Filon-type (see [17, 18, 27, 46, 64]), Levin-type methods (discussed below), Filon–Clenshaw–Curtis quadrature (see [15, 11]), 'double exponential formula' for Fourier-type integrals (see [49] and references therein). Reviews of the methods, their comparison and analysis, as well as bibliography notes can be found in [15, 28, 47, 25].

The first of two schemes developed in the present paper is based on the ideas of Levin, suggested in [33, 34]. The Levin method converts the calculation of an oscillatory integral into solving an ordinary differential equation (ODE) whose special, slowly oscillating solution is sought. Typically, the Chebyshev expansion is used as a representation of the solution and a collocation reduces the ODE to a system of linear equations. The Levin method has attracted much attention due to its ability to handle integrals with complicated phase functions, but the collocation has been found to be numerically unstable, leading to an ill-conditioned linear system for large number of nodes. Analysis and efforts to improve the stability of the Levin collocation method have been made, a number of Levin-type methods have been developed (see [15, 14, 28, 64, 35, 48, 36, 37] and references therein). Some progress has been achieved using careful analysis of the linear system and advanced methods of linear algebra such as TSVD (truncated singular value decomposition) and GMRES (generalized minimal residual) method. Our scheme is based on a different type of collocation — instead of the Chebyshev expansion we use a special form of Lagrange polynomial interpolation which was recently discovered as an effective tool for numerical analysis.

It is to note that polynomial interpolation formulae are widely used in theoretical studies, but not in numerical practice — in view of their instability. Finding the polynomials involves solution of a Vandermonde linear system of equations, which is exponentially unstable. Runge's phenomenon is also well known: for equispaced interpolation points small perturbations of the initial data may result in huge changes of the interpolant. However, it has been found (see [53, 23, 4, 57] and references therein) that these problems are avoided when using the Lagrange interpolation in one of the so-called barycentric forms and with the nodes clustered near the ends of the interval of approximation, e.g. at Chebyshev points. A review of the existing results and explanation of the attractive features of the barycentric Lagrange interpolation with a clustered set of nodes can be found in [4, 57]; rigorous confirmation of stability is given in [24].

Thus, in our first scheme, following [33, 34], we reduce evaluation of the integral in question to solution of an ODE on a finite interval. We prove that the ODE has one bounded solution and define the value of the function at the right end of the interval. Solution's value at the left end of the interval, up to a known factor, coincides with the sought value of the integral. To find the solution of the ODE numerically, we seek it in the form of a barycentric Lagrange interpolating polynomial (alternatively, the representation can include a term arising from an asymptotic analysis, intended to absorb 'bad' features of the solution such as sharp peaks). Then we apply collocation of the equation on a set of Chebyshev points. Our numerical experiments show that the constructed numerical algorithm is stable, typically converging steadily to the level of rounding errors with increase of the number of nodes, even in the presence of stationary points (which is considered as complication for Levin and Levin-type methods).

The second scheme, developed in the present paper, relies upon Clenshaw–Curtis quadrature [8] and the steepest descent method. First, we transform the integral contour along the steepest descent path in the complex plane and change variable to have a finite interval of integration. Further computation is based on the Clenshaw–Curtis quadrature, the method for numerical integration derived by an expansion of the integrand in terms of Chebyshev polynomials and approximation of the expansion coefficients using discrete Fourier transformation. The advantages of the quadrature rule are its fast convergence for smooth integrands at increasing number of nodes n (see [45, 56, 57]), naturally nested quadrature rules, effective computation of weights based on Fast Fourier Transform (see [20, 60]). So, the Clenshaw–Curtis quadrature shares the insensitivity of the FFT to rounding errors (see e.g. [30]) and the cost of implementation at $O(n \log n)$ operations. These properties of the quadrature, the simplicity and smoothness of the considered integrand suggest that in our particular case a 'brute-force' application of the quadrature can be fairly effective, which is confirmed by our numerical experiments. In the suggested scheme we build a sequence of approximations by increasing the number of quadrature's nodes (so that the number of intervals between nodes is doubled at each step) until some last values of the sequence become closer to each other than the given tolerance. Such simple estimate of the approximation error is known to be very realistic for the Clenshaw–Curtis integration (see [20]), which is also confirmed by our computations.

Using these two numerical algorithms we carry out evaluation of the wavelike term of the Green's function for a wide variety of parameters, comparing the accuracy of the approximations and their efficacy. These numerical experiments allow us to conclude that both developed algorithms are consistent, reliable and compatible in speed while the algorithm based on Levin ODE and barycentric Lagrange interpolation is somewhat faster when the order of interpolating polynomial, needed for achieving the given accuracy, is small (e.g. when the source or the field point is located sufficiently deeply). At the same time, the algorithm based on Clenshaw–Curtis quadrature works surprisingly well in the most difficult for the numerical integration zone, near the track of the source moving closely to the free surface.

We also consider application of the suggested methods to computation of derivatives of the wavelike term of the Green's function — the ability to compute the derivatives is fundamental in realization of many numerical methods (in particular, those based on integral equations of the potential theory). We show that generalization of both suggested numerical schemes is rather straightforward.

Now we give a brief outline of the paper. In § 2 we present the mathematical problem describing forward motion of a source and introduce a representation of the Green's function — the following sections are devoted to evaluation of its wavelike component. In § 3 we reduce evaluation of the integral to finding

a special solution of an ODE and study properties of the solution. In § 4 a numerical scheme based on the barycentric Lagrange interpolation is constructed for finding the solution of the differential equation. An alternative scheme for evaluation of the wavelike term, based on the steepest descent method and the Clenshaw–Curtis quadrature, is developed in § 5. In § 6 numerical experiments are carried out to test and compare the algorithms. Application of the suggested methods to computation of derivatives of the wavelike term is discussed in § 7. The paper concludes with a summary of the principal findings.

2 Statement of the problem and a representation of the Green function

Consider the mathematical problem for a velocity potential that describes the forward motion of a source with a constant speed U through an unbounded heavy fluid having a free surface F. The fluid is assumed to be ideal incompressible and having infinite depth; fluid's motion is irrotational and steady-state in a Cartesian coordinate system (x, y, z) attached to the source. The x-axis is parallel to the direction of motion, z is another horizontal axis, and y-axis is vertical and directed upwards. We will also use the notation $\boldsymbol{x} = (x, y, z)$. The source is located at $\boldsymbol{x}_0 = (x_0, y_0, z_0)$ so that the fluid fills in $W = \mathbb{R}^3_- \setminus \{\boldsymbol{x}_0\}$, where $\mathbb{R}^3_- = \{(x, z) \in \mathbb{R}^2,\ y < 0\}$, and $F = \partial\mathbb{R}^3_-$.

We consider the mathematical problem of the linear surface wave theory (often referred to as the Neumann–Kelvin problem — see book [31] and references therein). The motion of the source is described by a velocity potential $G(\boldsymbol{x}; \boldsymbol{x}_0) = G(x, y, z; x_0, y_0, z_0)$

$$-\nabla^2 G = \delta(x - x_0)\,\delta(y - y_0)\,\delta(z - z_0) \quad \text{when} \quad y \le 0, \quad y_0 < 0, \tag{1}$$

$$\partial_x^2 G + \nu \partial_y G = 0 \quad \text{when} \quad y = 0, \quad y_0 < 0, \tag{2}$$

where δ is Dirac's delta-function, $\nabla = (\partial_x, \partial_y, \partial_z)$, $\nu = g/U^2$ is the wave number, g denotes acceleration due to gravity.

Since the fluid domain is unbounded, the basic relations must be complemented with conditions prescribing behaviour of the potential at infinity (see [19, 13, 31, 41]). Following [41], we demand

$$\sup_{\mathbb{R}^3_- \setminus \{\boldsymbol{x}:\, |\boldsymbol{x} - \boldsymbol{x}_0| < r\}} |\nabla G| < \infty \quad \text{for some} \quad r > 0, \tag{3}$$

and

$$\iiint_{\{y<0,\ x>x_*\}} |\nabla G|^2 \,\mathrm{d}x\,\mathrm{d}y\,\mathrm{d}z < \infty \quad \text{for some} \quad x_* > x_0. \tag{4}$$

The latter condition is one of a few variants suggested in [41]. The statement (1)–(4) is proved in [41] to have a unique (up to an additive constant) solution.

Without loss of generality we can assume that $x_0 = 0$ and $z_0 = 0$. Further on we will assign the values and use the notation:

$$G(x, y, z; y_0) = G(x, y, z; 0, y_0, 0).$$

Besides, further we will use dimensionless coordinates by fixing $\nu = 1$.

A number of representations of the Green's function are known (see e.g. [63, 31] and references therein). Typically, they involve one double integral and one single integral. The single integral represents the far-field oscillatory part where one may recognize the well-known ship wake pattern, whilst the double integral mostly contributes to the local flow near the source. More suitable for numerical applications representations with the double integrals being transformed to single ones, have been derived (see [54, 44] and references therein). Further we use the formula suggested in [44]:

$$G(x, y, z; y_0) = -\frac{1}{4\pi R} + \frac{1}{4\pi R'} + I_0(x, y + y_0, z) + I_\infty(x, y + y_0, z).$$

Here $R = \sqrt{x^2 + (y - y_0)^2 + z^2}$, $R' = \sqrt{x^2 + (y + y_0)^2 + z^2}$, the 'near-field' term is written as follows:

$$I_0(x, y, z) = \frac{1}{2\pi^2} \operatorname{Im} \int_{-1}^{1} \mathrm{e}^{\xi(x,y,z,t)}\, E_1(\xi(x, y, z, t))\, \mathrm{d}t,$$

where $\xi(x, y, z, t) = y\big(1 - t^2\big) + \big(zt + \mathrm{i}|x|\big)\big(1 - t^2\big)^{1/2}$ and E_1 is the integral exponent function (see e.g. [1, § 5.1]). The integral representing the oscillating wavelike part of the Green function has the following form:

$$I_\infty(x, y, z) = \pi^{-1}\, H(-x) \operatorname{Im}\big\{I(x, y, z) + I(x, y, -z)\big\}. \tag{5}$$

Here H is Heaviside's function,

$$I(x, y, z) = \int_0^\infty \mathrm{e}^{\varpi(t,x,y,z)}\, \mathrm{d}t, \quad \text{where} \quad y < 0,\ x \le 0,\ z \in \mathbb{R}, \tag{6}$$
$$\varpi(t, x, y, z) = y\left(1 + t^2\right) + \mathrm{i}(x + zt)\sqrt{1 + t^2}.$$

Numerical evaluation of the function $I_0(x, y, z)$ is discussed in [43, 44, 42]. In the present work we are concerned with approximation of $I(x, y, z)$. Except the case $x = z = 0$ when $I = \frac{\sqrt{\pi}}{2}\frac{\mathrm{e}^y}{\sqrt{-y}}$, the problem is rather difficult because of the presence of two differently oscillating factors and the infinite interval of integration. For $z > 0$ and $x \le -2\sqrt{2}z$ there are also critical points $t^{\pm}_{\mathrm{crit}} = -\frac{x}{4z} \pm \sqrt{\left(\frac{x}{4z}\right)^2 - \frac{1}{2}}$ defined by the equation $2zt^2 + xt + z = 0$ ($\operatorname{Im}\{\varpi'_t\} = 0$), merging to one point when $x = -2\sqrt{2}z$.

3 Evaluation of the integral $I(x, y, z)$ based on an ordinary differential equation

In the section we shall apply the idea of [33] and reduce evaluation of the integral $I(\boldsymbol{x})$ defined by (6) to finding one special (bounded and slowly oscillatory) solution of an ordinary differential equation. For the convenience of the following numerical treatment we write $I(\boldsymbol{x})$ as an integral over the finite interval $(0, 1)$. By the change of variable $t = \tau/(1 - \tau)$ we have

$$I(\boldsymbol{x}) = \int_0^1 \frac{\mathrm{e}^{\varpi_*(\tau,\boldsymbol{x})}}{(1 - \tau)^2}\, \mathrm{d}\tau, \tag{7}$$

where $\varpi_*(\tau, \boldsymbol{x}) = \varpi(\tau/(1 - \tau), \boldsymbol{x})$. It is notable that, unlike the case considered in [33], there is the infinity of oscillations of the integrand in the neighborhood of $\tau = 1$ and the point needs a special attention.

Following [33], we write the identity

$$\left(\frac{\Psi(\tau)}{(1 - \tau)^2}\mathrm{e}^{\varpi_*(\tau,\boldsymbol{x})}\right)'_\tau = \frac{\mathrm{e}^{\varpi_*(\tau,\boldsymbol{x})}}{(1 - \tau)^2}\left[\Psi'(\tau) + \frac{2\,\Psi(\tau)}{1 - \tau} + \partial_\tau \varpi_*(\tau, \boldsymbol{x})\, \Psi(\tau)\right], \tag{8}$$

valid for an arbitrary differentiable function Ψ. Assume that we can find $\Psi(\tau) = \Psi(\tau, \boldsymbol{x})$ such that the expression in the square brackets in the last identity is equal to one. Then, obviously, we arrive at

$$I(\boldsymbol{x}) = \frac{\Psi(\tau, \boldsymbol{x})}{(1 - \tau)^2}\mathrm{e}^{\varpi_*(\tau,\boldsymbol{x})}\,\Big|_{\tau=0}^{\tau=1}.$$

The factors of Ψ in the expression in the square brackets in (8) are singular at $\tau = 1$, in particular, we have

$$\partial_\tau \varpi_*(\tau, \boldsymbol{x}) = \frac{\sigma(\tau, \boldsymbol{x})}{(1 - \tau)^3},$$

where

$$\sigma(\tau, \boldsymbol{x}) = \mathrm{i}x\frac{\tau(1 - \tau)}{\sqrt{2\tau^2 - 2\tau + 1}} + 2y\tau + \mathrm{i}z\frac{3\tau^2 - 2\tau + 1}{\sqrt{2\tau^2 - 2\tau + 1}}. \tag{9}$$

Therefore, assuming $|y+\mathrm{i}z|\neq 0$ (i.e. $\sigma(1,\boldsymbol{x})\neq 0$), it is convenient to define

$$\Psi(\tau,\boldsymbol{x})=(1-\tau)^3\,\Phi(\tau,\boldsymbol{x}).$$

Then, we are looking for $\Phi(\tau,\boldsymbol{x})$ satisfying on $[0,1]$ the following ordinary differential equation:

$$(1-\tau)^3\,\partial_\tau\Phi(\tau,\boldsymbol{x})+\left[\sigma(\tau,\boldsymbol{x})-(1-\tau)^2\right]\Phi(\tau,\boldsymbol{x})=1. \tag{10}$$

Further we will show that it is possible to find a particular solution to (10) that is bounded at $\tau=1$. (Solutions of this type arose in [33, 34], where they were named slowly oscillatory, — in our case the particular solution is also slowly oscillatory in comparison with the rapidly oscillatory solution to the homogeneous equation.) For the bounded solution, taking into account the definition of ϖ_*, we find

$$I(\boldsymbol{x})=-\,\Phi(0,\boldsymbol{x})\mathrm{e}^{y+\mathrm{i}x}. \tag{11}$$

Let us assume that $y<0$. It is not difficult to check that the general solution of (10) can be written in the following form:

$$\Phi^{\mathrm{gen}}(\tau,\boldsymbol{x})=c\frac{\mathrm{e}^{\Lambda(\tau,\boldsymbol{x})}}{\tau-1}+\Phi(\tau,\boldsymbol{x}), \tag{12}$$

where c is a constant,

$$\Lambda(\tau,\boldsymbol{x})=-(\tau-1)^{-2}\left(y+\mathrm{i}z\tau\sqrt{2\tau^2-2\tau+1}\right)-(\tau-1)^{-1}\left(2y-\mathrm{i}x\sqrt{2\tau^2-2\tau+1}\right), \tag{13}$$

$$\Phi(\tau,\boldsymbol{x})=\frac{\mathrm{e}^{\Lambda(\tau,\boldsymbol{x})}}{\tau-1}\int_\tau^1\frac{\mathrm{e}^{-\,\Lambda(\theta,\boldsymbol{x})}}{(\theta-1)^2}\,\mathrm{d}\theta. \tag{14}$$

The first term in the right-hand side of (12) is highly oscillating near $\tau=1$; besides, the amplitude of the oscillations grows when approaching $\tau=1$ (under the assumption $y<0$). So, we fix $c=0$ in (12) and consider the particular solution $\Phi(\tau,\boldsymbol{x})$.

From (13) we find

$$\begin{gathered}\Lambda(\tau,\boldsymbol{x})=\frac{\gamma_2}{(\tau-1)^2}+\frac{\gamma_1}{\tau-1}+\gamma_0+O(\tau-1),\quad\text{as}\quad\tau\to 1,\quad\text{where}\\ \gamma_2=-y-\mathrm{i}z,\quad\gamma_1=\mathrm{i}x-2y-2\mathrm{i}z,\quad\gamma_0=\mathrm{i}x-3\mathrm{i}z/2.\end{gathered} \tag{15}$$

Then we can write

$$\Phi(\tau,\boldsymbol{x})=\frac{\mathrm{e}^{\Lambda(\tau,\boldsymbol{x})}}{\tau-1}\int_\tau^1\frac{\mathrm{e}^{-\frac{\gamma_2}{(\theta-1)^2}-\frac{\gamma_1}{\theta-1}-\gamma_0}}{(\theta-1)^2}\,\Xi(\theta,\boldsymbol{x})\,\mathrm{d}\theta,$$

$$\Xi(\theta,\boldsymbol{x})=\exp\left\{-\Lambda(\theta,\boldsymbol{x})+\frac{\gamma_2}{(\theta-1)^2}+\frac{\gamma_1}{\theta-1}+\gamma_0\right\}=1+\rho(\theta,\boldsymbol{x}),$$

where $|\rho(\theta,\boldsymbol{x})|\le C(\boldsymbol{x})|\theta-1|$ for $\theta\in[0,1]$ and C is constant in θ. So, we have

$$\Phi(\tau,\boldsymbol{x})=\frac{\mathrm{e}^{\Lambda(\tau,\boldsymbol{x})}}{\tau-1}\left\{L_0(\tau,\boldsymbol{x})+\tilde{L}(\tau,\boldsymbol{x})\right\},\quad\text{where} \tag{16}$$

$$L_0(\tau,\boldsymbol{x})=\int_\tau^1(\theta-1)^{-2}\mathrm{e}^{-\frac{\gamma_2}{(\theta-1)^2}-\frac{\gamma_1}{\theta-1}-\gamma_0}\,\mathrm{d}\theta,\quad\tilde{L}(\tau,\boldsymbol{x})=\int_\tau^1\rho(\theta,\boldsymbol{x})(\theta-1)^{-2}\mathrm{e}^{-\frac{\gamma_2}{(\theta-1)^2}-\frac{\gamma_1}{\theta-1}-\gamma_0}\,\mathrm{d}\theta.$$

It is not difficult to find

$$L_0(\tau,\boldsymbol{x})=\frac{\sqrt{\pi}}{2\sqrt{\gamma_2}}\mathrm{e}^{-\gamma_0+\frac{\gamma_1^2}{4\gamma_2}}\operatorname{erfc}\left(\frac{\sqrt{\gamma_2}}{1-\tau}-\frac{\gamma_1}{2\sqrt{\gamma_2}}\right), \tag{17}$$

where we used change of variable $t = (1-\theta)^{-1}$, the equality $\gamma_2 t^2 - \gamma_1 t = \gamma_2 \left(t - \frac{\gamma_1}{2\gamma_2}\right)^2 - \frac{\gamma_1^2}{4\gamma_2}$, definitions of the error functions erf and erfc (see [1], 7.1.1, 7.1.2) and the fact that $\mathrm{erf}(\zeta) \to 1$ as $\zeta \to \infty$, $|\arg(\zeta)| < \pi/4$ ([1, 7.1.16]). Additionally, for $\tau \in [0,1]$ we have

$$|\tilde{L}(\tau, \boldsymbol{x})| \le C(\boldsymbol{x})(1-\tau) \int_\tau^1 \frac{\mathrm{e}^{\frac{y}{(\theta-1)^2} + \frac{2y}{\theta-1}}}{(\theta-1)^2} \mathrm{d}\theta = C(\boldsymbol{x})(1-\tau) \frac{\sqrt{\pi}}{2\sqrt{|y|}} \mathrm{e}^{-y} \mathrm{erfc}\left(\frac{\sqrt{|y|}\tau}{1-\tau}\right).$$

Then, a simple analysis based on the asymptotic expansion [1, 7.1.23] for the erfc function leads us to the estimate

$$\left| \frac{\mathrm{e}^{\Lambda(\tau,\boldsymbol{x})}}{\tau - 1} \tilde{L}(\tau, \boldsymbol{x}) \right| = O\big(\tau - 1\big) \quad \text{as} \quad \tau \to 1 - 0. \tag{18}$$

Taking into account (16), (17), (18) and using the expansion [1, 7.1.23] we find

$$\begin{gathered} \Phi(\tau, \boldsymbol{x}) = \Phi(1, \boldsymbol{x}) + O(\tau - 1), \quad \text{as} \quad \tau \to 1 - 0, \quad \text{where} \\ \Phi(1, \boldsymbol{x}) := \lim_{\tau \to 1-0} \Phi(\tau, \boldsymbol{x}) = \frac{1}{2(y + \mathrm{i}z)}. \end{gathered} \tag{19}$$

Thus, we have also presented the boundary condition that characterizes the bounded and slowly oscillating solution of (10).

4 Numerical solution of (10), (19)

In this section we will be concerned with finding numerical solution of (10), (19). At this we will consider $\boldsymbol{x}$ as a fixed parameter and for brevity in many cases we will avoid explicit denoting of the dependence on $\boldsymbol{x}$ for Φ and some other values.

Obviously, for finding solution to (10), (19) one can try to apply standard ODE solvers. We have tested the built-in subroutines of the used in the present work numerical computing environment GNU Octave and the subroutines provided by `odepkg` package to solve stiff differential-algebraic equations. Amidst these subroutines, the most reliable and applicable for the widest range of parameters (x, y, z) was `ode5r`, which is a realization of the RADAU5 solver [22], using an implicit Runge–Kutta method of order 5 with step size control. For application of the subroutine, the equation (10) was transformed to a system of the form $\boldsymbol{M}\,(\Phi', \Psi')^{\mathsf{T}} = \boldsymbol{f}(\Phi, \Psi)$ with degenerate but constant matrix $\boldsymbol{M}$ in the left-hand side. (Here and below the symbol $^{\mathsf{T}}$ means transposition.) Namely, we use the system

$$\begin{cases} \Psi' = 1 - \big[2(1-\tau)^2 + \sigma(\tau, x, y, z)\big]\,\Phi, \\ 0 = \Psi - (1-\tau)^3 \Phi, \end{cases}$$

with the boundary conditions $\Psi(1) = 0$, $\Phi(1) = 1/(2(y + \mathrm{i}z))$. We denote by $I_\varepsilon^{\mathrm{R5}}(x, y, z)$ the corresponding approximation of $I(x, y, z)$ found with (11); here ε is the accuracy demanded from the subroutine `ode5r`. Comparing to other methods developed in the present paper for evaluation of $I(\boldsymbol{x})$, the main disadvantage of `ode5r` solver is its being rather slow for the particular problem. The subject will be shortly addressed in § 6, but generally we will not discuss details of application of standard solvers to (10), (19).

In the numerical algorithm developed in the present section we seek the solution to (10) in the form of a polynomial $\Phi_M(\tau)$ of the order M. This, obviously, excludes from (12) the rapidly oscillatory unbounded solutions of the homogeneous equation and allows us to find an approximation of $\Phi(\tau)$, given by (14), avoiding explicit usage of the condition (19). For a discretization of the differential equation and reduction it to a linear system we use a collocation scheme demanding that $\Phi_M(\tau)$ satisfies (10) at the following set of Chebyshev points on the interval $[0, 1]$:

$$\tau_k = (1 - \cos(k\pi/M))/2, \quad k = 0, 1, ..., M. \tag{20}$$

We write $\Phi_M(\tau)$ as a Lagrange interpolating polynomial so that the values $\Phi_M(\tau_k) \approx \Phi(\tau_l)$ are unknowns of the linear system. Although polynomial interpolations are usually avoided in numerical practice, recently (see [4, 57, 24]) it was noted that the Lagrange interpolation is highly effective and numerically stable when the polynomial is manipulated through the formulas of barycentric interpolation and the nodes are clustered near the ends of the interval of approximation, in particular, as for Chebyshev points.

So, an approximation of the solution to (10), (19) is sought in the form of the barycentric Lagrange interpolating polynomial:

$$\Phi_M(\tau) = \sum_{m=0}^{M} \ell_m(\tau)\, \Phi_m, \tag{21}$$

$$\ell_m(\tau) = \frac{\omega_m}{\tau - \tau_m} \Big/ \sum_{k=0}^{M} \frac{\omega_k}{\tau - \tau_k}, \quad \omega_k = \left[\prod_{l=0,\, l\neq k}^{M} (\tau_k - \tau_l) \right]^{-1}, \quad k, m = 0, 1, ..., M. \tag{22}$$

By construction $\Phi_l = \Phi_M(\tau_l)$, $l = 0, 1, ..., M$. For the set of the Chebyshev points $\{\tau_k\}$, defined by (20), expressions for ω_k are found in [53]. Cancelling factors independent of k we write

$$\omega_k = (-1)^k \varsigma_k, \quad \varsigma_k = \begin{cases} 1, & k = 1 \text{ or } k = M, \\ 2, & \text{otherwise.} \end{cases}$$

Using (22) we write the following expression

$$\ell'_m(\tau) = \frac{\omega_m}{(\tau - \tau_m)} \sum_{k=0}^{M} \frac{\omega_k}{(\tau - \tau_k)^2} \left[\sum_{k=0}^{M} \frac{\omega_k}{\tau - \tau_k} \right]^{-2} - \frac{\omega_m}{(\tau - \tau_m)^2} \left[\sum_{k=0}^{M} \frac{\omega_k}{\tau - \tau_k} \right]^{-1}. \tag{23}$$

In view of (23) it is not difficult to find

$$\ell'_m(\tau_l) = \begin{cases} \dfrac{\omega_m}{\omega_l(\tau_l - \tau_m)} & \text{for } m \neq l, \\ \displaystyle\sum_{k=0,\, k\neq m}^{M} \frac{\omega_k}{\omega_m(\tau_k - \tau_m)} & \text{for } \ m = l. \end{cases}$$

This, obviously, results in the formula

$$\Phi'_M(\tau_l) = \sum_{k=0,\, k\neq l}^{M} \frac{\omega_k}{\omega_l(\tau_k - \tau_l)} \left[\Phi_l - \Phi_k \right]. \tag{24}$$

Further we substitute (21), (24) into (10) and demand the equality to hold at the points τ_k, $k = 0, 1, ..., M$. In this way we arrive at the linear system

$$\boldsymbol{A}\boldsymbol{\Phi} = \boldsymbol{b}, \tag{25}$$

where $\boldsymbol{\Phi} = (\Phi_0, \Phi_1, ..., \Phi_M)^{\mathsf{T}}$ and $\boldsymbol{b} = (1, 1, ..., 1)^{\mathsf{T}}$. To write an expression of the matrix $\boldsymbol{A}$ we define $\mathring{\boldsymbol{A}} = [\mathring{a}_{ij}]_{i,j=0}^{M}$, where $\mathring{a}_{ii} = 0$ and $\mathring{a}_{ij} = -\omega_j/(\omega_i(\tau_j - \tau_i))$. Let also $s_i = \sum_{j=0}^{M} \mathring{a}_{ij}$, $i = 0, 1, ..., M$. Then, we have $\boldsymbol{A} = \operatorname{diag}\{(1 - \boldsymbol{\tau})^3\} \cdot \big(\mathring{\boldsymbol{A}} - \operatorname{diag}\{s_0, s_1, ..., s_M\}\big) + \operatorname{diag}\{\sigma(\boldsymbol{\tau}, x, y, z) - (1 - \boldsymbol{\tau})^2\}$.

Finally, we solve the linear system (25) and in accordance with (11) the approximation of the sought value of (6) by the scheme based on Levin's equation and Lagrange interpolation is as follows

$$I(x, y, z) \approx I_M^{\text{L–L}}(x, y, z) := -\Phi_0 \mathrm{e}^{y + \mathrm{i}x}. \tag{26}$$

Here is a Matlab (Octave) code of a function finding this approximation:

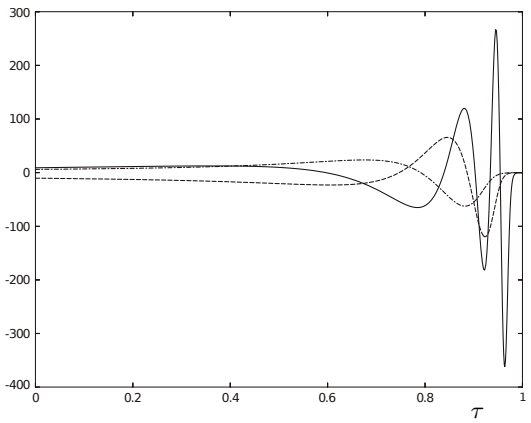

Figure 1: The graph of $\mathrm{Re}\{\Phi(\tau)\}$ for $x=-1$, $y=0$, $z=0.015$ (solid line), $z=0.03$ (dashed line), $z=0.045$ (dash-dotted line).

```
function res = Iapprox(x,y,z,M)
  sigma = @(tau,x,y,z) 2*y*tau + 1i*(x*tau.*(1-tau)+z*(3*tau.^2-2*tau+1)) ...
   ./sqrt(2*tau.^2-2*tau+1);
  tau = (1-cos(pi*(0:M)'/M))/2; w = [1; 2*ones(M-1,1); 1].*(-1).^((0:M)');
  A0 = -repmat(w',M+1,1)./repmat(w,1,M+1)./(repmat(tau',M+1,1)-repmat(tau,1,M+1));
  A0(1:(M+2):end) = 0;  A0 = A0 - diag(sum(A0,2));
  A = diag((1-tau).^3)*A0 + diag(sigma(tau,x,y,z)-(1-tau).^2);
  Phi = A\ones(M+1,1);
  res = -exp(y+1i*x) * Phi(1);
end
```

To improve the above scheme we can seek the solution to (10), (19) in the form

$$\Phi(\tau) \approx \hat{\phi}(\tau) + \Phi_M(\tau), \tag{27}$$

where $\Phi_M(\tau)$ is defined by (21) and $\hat{\phi}$ is a function that is intended to absorb some irregularities in behaviour of Φ (like sharp peaks). As shown in fig. 1, in particular, the irregular behaviour is characteristic when $y=0$, $z>0$ and the point (x,y,z) approaches $(x,0,0)$ (track behind the source located on the free surface). The peaks concentrate near the critical value $\tau_* = \big(2z - x + \sqrt{x^2-8z^2}\big)/(6z-2x)$, where $\mathrm{Im}\{\sigma(\tau_*,\boldsymbol{x})\}=0$.

Since τ_* is close to 1 when z is small, we will use the representation (16) and in view of (15) we define

$$\hat{\phi}(\tau) = \frac{\mathrm{e}^{\frac{\gamma_2}{(\tau-1)^2}+\frac{\gamma_1}{\tau-1}+\gamma_0}}{\tau-1}\, L_0(\tau,\boldsymbol{x}).$$

It is convenient to rewrite the last formula in terms of Faddeeva function $\mathrm{w}(\eta) = \mathrm{e}^{-\eta^2}\mathrm{erfc}(-\mathrm{i}\eta)$ [16]. By a simple algebra we find

$$\hat{\phi}(\tau) = \frac{\sqrt{\pi}}{2(\tau-1)\sqrt{\gamma_2}}\,\mathrm{w}\left(\frac{\mathrm{i}\sqrt{\gamma_2}}{1-\tau} - \frac{\mathrm{i}\gamma_1}{2\sqrt{\gamma_2}}\right). \tag{28}$$

The last function can be effectively evaluated using known algorithms and packages (e.g. [29]).

By using (27) we arrive at the linear system (25) with another right-hand side:

$$\boldsymbol{b}^* = (1,1,...,1)^{\mathsf{T}} - \boldsymbol{\ell}, \tag{29}$$

where $\boldsymbol{\ell} = \big(\hat{L}(\tau_0), \hat{L}(\tau_1), ..., \hat{L}(\tau_M)\big)^{\mathsf{T}}$,

$$\hat{L}(\tau) = \mathcal{L}\,\hat{\phi}(\tau) = (1-\tau)^3\,\hat{\phi}'(\tau) + \big[\sigma(\tau,x,y,z) - (1-\tau)^2\big]\,\hat{\phi}(\tau)$$
$$= 1 + \frac{\sqrt{\pi}}{2\sqrt{y+\mathrm{i}z}(\tau-1)}\left\{\frac{\big(3\tau^2-2\tau+1\big)z + \tau(1-\tau)x}{\sqrt{2\tau^2-2\tau+1}} - 2\tau z + (\tau-1)x\right\}\mathrm{w}\left(\frac{\tau\sqrt{y+\mathrm{i}z}}{\tau-1} - \frac{\mathrm{i}x}{2\sqrt{y+\mathrm{i}z}}\right). \tag{30}$$

Further we shall denote by $\hat{I}_M^{\text{L–L}}(x,y,z)$ the approximation of $I(x,y,z)$ obtained with the help of (27) and (28). Practically, $\hat{I}_M^{\text{L–L}}(x,y,z)$ has advantages comparing with $I_M^{\text{L–L}}(x,y,z)$ when τ_* is close to 1.

It is also useful to have a way to control errors of the approximation. After solving the system (25), by using (21) and defining $\Phi'_M(\tau)$ with the help of (23) we can find the residual $r(\tau)$ of the equation (10) ($r = \mathcal{L}\Phi_M - 1$). Analogously, if we solve the system $\boldsymbol{A\Phi} = \boldsymbol{b}^*$, where $\boldsymbol{b}^*$ is given by (29), then the residual of the equation (10) is defined by $r = \mathcal{L}\big(\Phi_M + \hat{\phi}\big) - 1$. At this, the residual of the solution $R = \Phi_M - \Phi$ (or $R = \Phi_M + \hat{\phi} - \Phi$) satisfies the equation

$$\mathcal{L}R = r. \tag{31}$$

Since $R(\tau)$ is the slowly oscillating, bounded solution to (31), following arguments of § 3, we find

$$R(\tau) = \frac{\mathrm{e}^{\Lambda(\tau)}}{\tau-1}\int_\tau^1 \frac{r(\theta)\mathrm{e}^{-\Lambda(\theta)}}{(\theta-1)^2}\,\mathrm{d}\theta, \tag{32}$$

where Λ is defined in (13). The representation (32) allows us to obtain a simple estimates of $\big|I - I_M^{\text{L–L}}\big|$ and $\big|I - \hat{I}_M^{\text{L–L}}\big|$ if $y < 0$. Namely, fixing $\tau = 0$ in (32) and taking into account (11), (13), (26) we find

$$\big|I - I_M^{\text{L–L}}\big| \le \mathrm{e}^{2y}\left|\int_0^1 \frac{r(\theta)\mathrm{e}^{-\Lambda(\theta,\boldsymbol{x})}}{(1-\theta)^2}\,\mathrm{d}\theta\right| \le \mathrm{e}^{2y}\max_{\theta\in[0,1]}\{|r(\theta)|\}\int_0^1 \frac{\mathrm{e}^{\frac{y}{(\theta-1)^2}+\frac{2y}{\theta-1}}}{(\theta-1)^2}\mathrm{d}\theta = \frac{\sqrt{\pi}}{2\sqrt{|y|}}\mathrm{e}^{y}\max_{\theta\in[0,1]}\{|r(\theta)|\}. \tag{33}$$

This estimate also holds for $\big|I - \hat{I}_M^{\text{L–L}}\big|$. In practice, it is convenient to compute $r_k = r(\check{\tau}_k)$ at $\check{M} = M - 1$ Chebyshev points

$$\check{\tau}_k = \frac{1}{2}\left(1 - \cos\left(\frac{(k+1/2)\pi}{\check{M}+1}\right)\right), \quad k = 0, 1, ..., \check{M}.$$

At this $\check{\tau}_k \in (\tau_k, \tau_{k+1})$ and taking into account the nature of $r(\tau)$ which oscillates between zero values at τ_k, we can assume that $\max_{k=0,1,...,M}\{|r_k|\}$ approximates the term $\max_{\theta\in[0,1]}\{|r(\theta)|\}$ in the right-hand side of (33).

Unfortunately, the estimate (33) is poor for small $|y|$. In this case we can use the following approach. We approximate $R(\tau)$ by

$$R_{\check{M}}(\tau) = \sum_{m=0}^{\check{M}} \check{\ell}_m(\tau)\,R_m, \tag{34}$$

where $\check{\ell}_m(\tau)$ is computed analogously to (22), for $\check{\tau}_k$ and $\check{\omega}_k$ defined as follows (see e.g. [4]):

$$\check{\omega}_k = (-1)^k \sin\big((k+1/2)\pi/\big(\check{M}+1\big)\big), \quad k = 0, 1, ..., \check{M}.$$

Substituting (34) and the corresponding representation of $R'_{\check{M}}$ (see (24)) into (31) we demand the equality to hold at the points $\check{\tau}_k$, $k = 0, 1, ..., \check{M}$. In this way we obtain the linear system

$$\boldsymbol{BR} = \boldsymbol{r}, \tag{35}$$

where $\boldsymbol{R} = (R_0, R_1, ..., R_{\check{M}})^{\mathsf{T}}$, $\boldsymbol{r} = (r_0, r_1, ..., r_{\check{M}})^{\mathsf{T}}$. Defining $\mathring{\boldsymbol{B}} = \big[\mathring{b}_{ij}\big]_{i,j=0}^{\check{M}}$, $\mathring{b}_{ii} = 0$, $\mathring{b}_{ij} = -\check{\omega}_j/(\check{\omega}_i(\check{\tau}_j - \check{\tau}_i))$ and $\check{s}_i = \sum_{j=0}^{\check{M}} \mathring{b}_{ij}$, we have $\boldsymbol{B} = \operatorname{diag}\big\{(1-\check{\boldsymbol{\tau}})^3\big\} \cdot \big(\mathring{\boldsymbol{B}} - \operatorname{diag}\{\check{s}_0, \check{s}_1, ..., \check{s}_M\}\big) + \operatorname{diag}\{\sigma(\check{\boldsymbol{\tau}}, x, y, z) - (1-\check{\boldsymbol{\tau}})^2\big\}$.

We solve the system (35) and assume that $|R(0)| \le \|\boldsymbol{R}\|_\infty = \max\{|R_k| : k = 0, 1, ..., \check{M}\}$ (assumption $|R(0)| \le |R_0|$ would be more accurate but less reliable choice). Finally, we can estimate $\big|I - I_M^{\text{L–L}}\big|$ and $\big|I - \hat{I}_M^{\text{L–L}}\big|$ by the value

$$\varepsilon_M^{\text{L–L}}(x, y, z) = \mathrm{e}^y \min\Big\{\|\boldsymbol{R}\|_\infty, 2^{-1}(\pi/|y|)^{1/2}\|\boldsymbol{r}\|_\infty\Big\}. \tag{36}$$

Our numerical experiments (see § 6) show that the estimate $\varepsilon_M^{\text{L–L}}$ is rather reliable. However, evaluation of $\varepsilon_M^{\text{L–L}}$ is time-consuming, so in § 6 we also discuss ways to avoid the computations.

5 Evaluation of $I(x, y, z)$ based on Clenshaw–Curtis quadrature and steepest descent method

Another scheme, developed in the present work to compute $I(x, y, z)$, is based on application of Clenshaw–Curtis quadrature where, as a preliminary, we use the steepest descent method. (It is notable that the latter method could be used to improve the scheme of § 3, 4.)

For the function $\varpi(t, x, y, z)$ involved in the definition of $I(x, y, z)$ by (6), we have

$$\varpi(t, x, y, z) = (y + \mathrm{i}z)t^2 + \mathrm{i}xt + y + O\big(t^{-1}\big) \quad \text{as} \quad t \to \infty. \tag{37}$$

Therefore, Jordan's lemma allows rotation $t \to \mathrm{e}^{\mathrm{i}\theta}t$ of the integration contour in (6) if $\operatorname{Re}\big[(y + \mathrm{i}z)\mathrm{e}^{2\mathrm{i}\vartheta}\big] < 0$ for $\vartheta \in (0, \theta)$. The value of θ corresponding to the steepest descent for sufficiently large t can be found by minimizing $\operatorname{Re}\big[(y + \mathrm{i}z)\mathrm{e}^{2\mathrm{i}\theta}\big]$. This gives

$$\begin{gathered}\cos 2\theta = \frac{-y}{\sqrt{y^2+z^2}}, \quad \sin 2\theta = \frac{z}{\sqrt{y^2+z^2}}, \quad \operatorname{Re}\big[(y + \mathrm{i}z)\mathrm{e}^{2\mathrm{i}\theta}\big] = -\sqrt{y^2+z^2}, \\ \cos\theta = \sqrt{\frac{1 + |y|/\sqrt{y^2+z^2}}{2}}, \quad \sin\theta = \operatorname{sign}(z)\sqrt{\frac{1 - |y|/\sqrt{y^2+z^2}}{2}}.\end{gathered} \tag{38}$$

We note that $\operatorname{sign}(z)\,\theta \in [0, \frac{\pi}{4}]$. Therefore, for $z < 0$, $\operatorname{Re}\big[\mathrm{i}x\mathrm{e}^{\mathrm{i}\theta}\big] < 0$ and after the rotation the second term in the right-hand side of (37) provides the decaying exponential factor $\exp\{-xt\sin\theta\}$ in the integrand as $t \to \infty$. Hence, for $z \le 0$ we will use the following expression:

$$I(x, y, z) = \mathrm{e}^{\mathrm{i}\theta} \int_0^\infty \mathrm{e}^{\varpi(\mathrm{e}^{\mathrm{i}\theta}t, x, y, z)}\,\mathrm{d}t. \tag{39}$$

The case $z > 0$ needs more attention, because then $\operatorname{Re}\big[\mathrm{i}x\mathrm{e}^{\mathrm{i}\theta}\big] > 0$ and the second term in the right-hand side of (37) prevails in some finite interval of $t \ge 0$. So, the definition (39) would not be useful for numerical computations due to the presence of very large (in absolute magnitude) values of the integrand. Therefore, we split the interval of integration into two parts and write

$$I(x, y, z) = \int_0^{t_*} \mathrm{e}^{\varpi(t, x, y, z)}\,\mathrm{d}t + \mathrm{e}^{\mathrm{i}\theta} \int_0^\infty \mathrm{e}^{\varpi(\gamma(t), x, y, z)}\,\mathrm{d}t, \tag{40}$$

where $\gamma(t) = t_* + t\mathrm{e}^{\mathrm{i}\theta}$. We need the real part of $\varpi(\gamma(t), x, y, z)$ to be negative for $t \ge 0$. Looking at (37), to find t_* we demand that for $t \ge 0$

$$|x|\operatorname{Im}(\gamma(t)) \le z\operatorname{Im}\big([\gamma(t)]^2\big) + |y|\big[1 + \operatorname{Re}\big([\gamma(t)]^2\big)\big]. \tag{41}$$

By using (38) we rewrite the right-hand side of the latter inequality as follows:

$$2tt_*\left(|y|\cos\theta + z\sin\theta\right) + t^2\sqrt{y^2+z^2} + |y|\left(1 + t_*^2\right).$$

Thus, it is easy to find that the inequality (41) holds for $t \geq 0$ if $|x|\,\mathrm{Im}(\gamma(t)) \leq 2tt_*\,(|y|\cos\theta + z\sin\theta)$. Thus, in our computations we fix

$$t_* = \frac{|x|\sin\theta}{2(|y|\cos\theta + z\sin\theta)}. \tag{42}$$

To find approximation of the integrals in (39), (40) we will use the Clenshaw–Curtis quadrature [8]. First we give an outline of the method emphasizing the possibility of effective application of the quadrature using FFT. Consider the integral

$$\int_{-1}^{1} f(t)\,\mathrm{d}t \tag{43}$$

for some function $f : [-1, 1] \mapsto \mathbb{R}$. Expand the function f into the series of Chebyshev polynomials:

$$f(t) = \sum_{k=0}^{\infty} \epsilon_k c_k\, T_k(t), \tag{44}$$

where $\epsilon_0 = 1/2$, $\epsilon_k = 1$, $k \geq 1$, $T_k(t) = \cos(k\arccos(t))$. Then, it can be found that

$$\int_{-1}^{1} f(t)\,\mathrm{d}t = c_0 + 2\sum_{k=1}^{\infty} \frac{c_{2k}}{1-(2k)^2} = d_0 + 2\sum_{k=1}^{\infty} \frac{d_k}{1-(2k)^2}, \tag{45}$$

where we define $d_k = c_{2k}$, $k = 0, 1, 2, ...$ In view of the definition $T_k(t)$, the change $t = \cos(\tau)$ in (44) and the orthogonality of the cosines in $L_2(0, \pi)$ lead us to

$$d_k = \frac{2}{\pi}\int_0^{\pi} f(\cos\tau)\cos(2k\tau)\,\mathrm{d}\tau.$$

Let us now fix a sufficiently large, even integer N and use the trapezoidal rule to approximate the latter integral:

$$d_k \approx \delta_k = \frac{2}{N}\left[\frac{f(1)}{2} + \frac{f(-1)}{2} + \sum_{n=1}^{N-1} f(\cos(n\pi/N))\cos(2\pi nk/N)\right]. \tag{46}$$

It is easy to note that (46) expresses δ_k through the discrete Fourier transform that maps one vector of length N (say, $\boldsymbol{u}$) to another one (say, $\boldsymbol{U}$) via $U_{k,N} = \sum_{n=0}^{N-1} u_n \mathrm{e}^{-\mathrm{i}2\pi kn/N}$. We write $\boldsymbol{U} = \mathcal{F}(\boldsymbol{u})$ or, equivalently, in the matrix notation $\boldsymbol{U} = \boldsymbol{F}\boldsymbol{u}$, where $\boldsymbol{F} = [\phi_{\alpha\beta}]_{\alpha,\beta=1}^{N}$, $\phi_{\alpha\beta} = \mathrm{e}^{-2\pi\mathrm{i}(\alpha-1)(\beta-1)/N}$. Then, we have

$$\boldsymbol{\delta} = (\delta_0, \delta_1, ..., \delta_{N-1})^{\mathsf{T}} = \frac{2}{N}\,\mathrm{Re}\{\boldsymbol{F}\}\boldsymbol{f}_*, \tag{47}$$

where $\boldsymbol{f}_* = ([f(1) + f(-1)]/2, f(t_{1,N}), ..., f(t_{N-1,N}))^{\mathsf{T}}$, $t_{k,N} = \cos k\pi/N$ are extrema of $T_N(t)$.

We note that $\delta_{\frac{N}{2}+\ell} = \delta_{\frac{N}{2}-\ell}$, $\ell = 1, 2, ..., N/2 - 1$, and define the vector $\boldsymbol{\kappa} = (1, \kappa_1, ..., \kappa_{N-1})^{\mathsf{T}}$, such that $\kappa_n = 1/\big(1-4n^2\big)$ for $n = 1, 2, ..., N/2$ and $\kappa_n = 1/\big(1-4(N-n)^2\big)$ for $n = N/2+1, N/2+2, ..., N-1$. Then, in view of (45), (46) and (47) we can write

$$\int_{-1}^{1} f(t)\,\mathrm{d}t \approx \delta_0 + 2\sum_{k=1}^{N/2} \frac{\delta_k}{1-4k^2} = \boldsymbol{\kappa}^{\mathsf{T}}\boldsymbol{\delta} = \frac{2}{N}\boldsymbol{\kappa}^{\mathsf{T}}\,\mathrm{Re}\{\boldsymbol{F}\}\boldsymbol{f}_* = \frac{2}{N}\big(\mathrm{Re}\{\boldsymbol{F}\}\boldsymbol{\kappa}\big)^{\mathsf{T}}\boldsymbol{f}_*,$$

where we use the fact that $\mathrm{Re}\{\boldsymbol{F}\}$ is symmetric. Finally, we find

$$\int_{-1}^{1} f(t)\,\mathrm{d}t \approx \boldsymbol{v}^{\mathsf{T}}\boldsymbol{f}_* = \boldsymbol{w}^{\mathsf{T}}\boldsymbol{f}, \tag{48}$$

where $\boldsymbol{v} = \frac{2}{N}\,\mathrm{Re}\{\boldsymbol{F}\}\boldsymbol{\kappa} = \frac{2}{N}\,\mathrm{Re}\{\mathcal{F}(\boldsymbol{\kappa})\}$ and the second equality is the usual form of a quadrature with weights $\boldsymbol{w} = (2^{-1}v_0, v_1, ..., v_{N-1}, 2^{-1}v_0)^{\mathsf{T}}$ and values of the integrand $\boldsymbol{f} = \big(f(t_{0,N}), f(t_{1,N}), ..., f(t_{N,N})\big)^{\mathsf{T}}$. The weights $\boldsymbol{v}$ and $\boldsymbol{w}$ can be effectively computed using FFT. (Applicability of FFT for calculation of weights of Clenshaw–Curtis quadrature was first pointed out in [20].) So, the quadrature shares the usual excellent numerical stability of the FFT (see e.g. [30]) and the low cost of implementation.

Further we transform the integrals in (39), (40), where t_* is defined by (42), to integrals over $[-1, 1]$ of the type (43) by the following changes of variables

$$\begin{aligned} \int_0^{t_*} q(t)\,\mathrm{d}t &= \frac{t_*}{2}\int_{-1}^{1} q\left(\frac{t_*(t+1)}{2}\right)\,\mathrm{d}t = \int_{-1}^{1} f(t)\,\mathrm{d}t, \\ \int_0^{\infty} q(t)\,\mathrm{d}t &= 2\int_{-1}^{1} (1-t)^{-2}\, q\left(\frac{t+1}{1-t}\right)\,\mathrm{d}t = \int_{-1}^{1} f(t)\,\mathrm{d}t, \end{aligned} \tag{49}$$

Consider any one of the integrals arising in (39), (40) after the change of variables (49). We introduce the notation

$$\mathring{F}_N(f) = \boldsymbol{w}^{\mathsf{T}}\boldsymbol{f} \tag{50}$$

for the approximation obtained through (48). It is easy to note that for $y^2+z^2 \neq 0$ the function f in question is absolutely continuous on $[-1, 1]$ along with all derivatives $f^{(k)}$, $k = 1, 2, ...$ Thus, by Theorem 5.1 [56] for any integer $k > 0$ and all sufficiently large N

$$\rho_N := \left|\mathring{F}_N(f) - \int_{-1}^{1} f(t)\,\mathrm{d}t\right| \leq CN^{-k}, \tag{51}$$

where the constant C depends on f and k.

We will apply the approximation (50) in a 'brute force' manner, increasing N until we are sure that $\rho_N \leq \varepsilon$ for the given accuracy ε. The reasons, why one can expect to obtain a relatively effective scheme in this way, are the guaranteed by (51) convergence of the sequence $\mathring{F}_N = \mathring{F}_N(f)$ to its limit value as $N \to \infty$; the insensitivity of Clenshaw–Curtis scheme to rounding errors in the evaluation of the integrand; low ($N\log(N)$) cost of implementation and simplicity of the integrand. As we shall see in § 6, the suggested numerical approach works rather well even sufficiently close to the line $y = 0$, $z = 0$.

Since the Clenshaw–Curtis quadrature is naturally nested, in order not to waste already computed integrand values when computing the sequence $\{\mathring{F}_N\}$, it is convenient to choose the next step value of N to be a multiple of the previous one. Hence we will consider $F_\ell = \mathring{F}_{2^\ell N_0}$, $\ell = 0, 1, 2, ...$, for some initial even integer N_0 (in computations, presented in § 6, $N_0 = 2$).

A number of estimates for ρ_N have been proposed — see [20, 21] and references therein. We shall use the simple error estimate, demanding convergence of F_ℓ as a Cauchy sequence — so that the computation is stopped at the step $\ell = \ell_*$ if the last # members of the sequence $\{F_\ell\}$ are sufficiently close to each other: $\max\{|F_{\ell_*-i+1} - F_{\ell_*-j+1}| : 1 \leq i \leq \#,\, 1 \leq j \leq \#\} \leq \varepsilon$. It is known that for rapidly convergent processes such estimate can be rough, essentially overestimating the error. However, as it is emphasized in [20] the considerable experience of implementation of the Clenshaw–Curtis scheme confirms that the simple estimate is very realistic. The conclusion agrees with the observations made in the present work.

In our computations, presented in the next section, # = 3 and we also introduce the reserve coefficient $c_r = 10$ for the difference of F_{ℓ_*} and F_{ℓ_*-1}, so that the termination condition is as follows:

$$\max\left\{c_r\,|F_{\ell_*} - F_{\ell_*-1}|, |F_{\ell_*} - F_{\ell_*-2}|, |F_{\ell_*-1} - F_{\ell_*-2}|\right\} \leq \varepsilon. \tag{52}$$

Further we will denote by $I_\varepsilon^{\text{C–C}}(x, y, z)$ the approximation of $I(x, y, z)$ obtained with the help of (39), (40), (48), (49), (50) and (52). We also denote by $\mathcal{N}_\varepsilon^{\text{C–C}}(x, y, z)$ the total number of evaluations of the functions under integral signs in (39) or (40), needed to satisfy (52). For $z \leq 0$, when we use the expression (39), $\mathcal{N}_\varepsilon^{\text{C–C}}(x, y, z) = 2^{\ell_*}N_0 + 1$; for $z > 0$, $\mathcal{N}_\varepsilon^{\text{C–C}}(x, y, z) = \left(2^{\ell'_*} + 2^{\ell''_*}\right)N_0 + 2$, where ℓ'_* (ℓ''_*) is such that (52) holds for the first (second) integral in the right-hand side of (40).

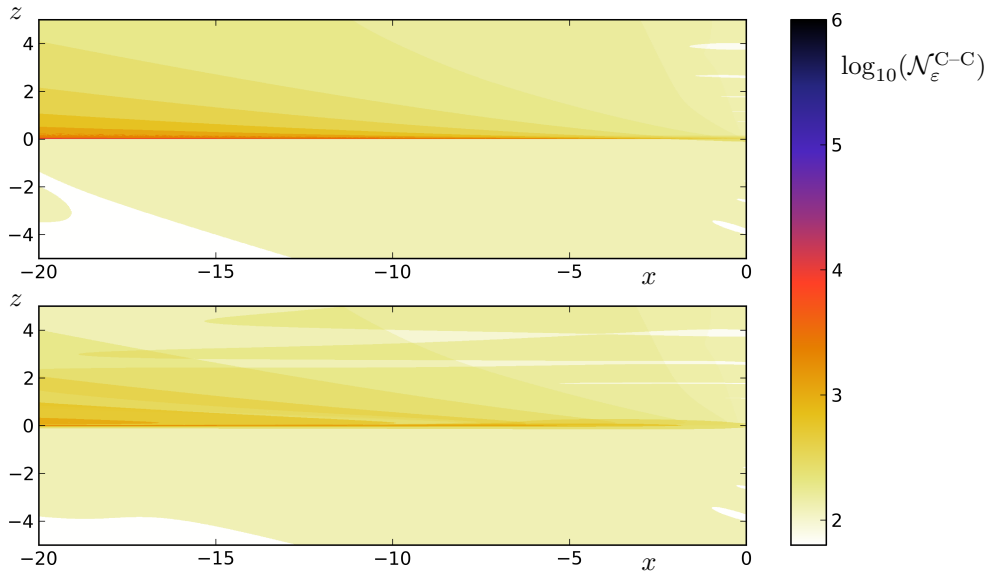

Figure 2: Values of $\log_{10}\bigl(\mathcal{N}_\varepsilon^{\mathrm{C-C}}(x,y,z)\bigr)$ for $\varepsilon = 10^{-6}$ and $y = 0$ (upper), $y = -0.1$ (lower).

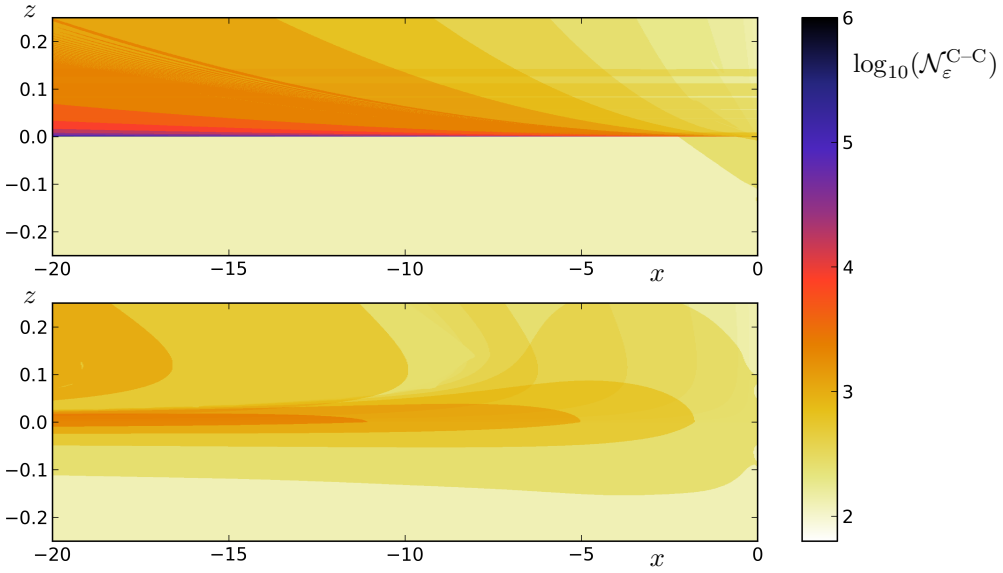

Figure 3: Values of $\log_{10}\bigl(\mathcal{N}_\varepsilon^{\mathrm{C-C}}(x,y,z)\bigr)$ for $\varepsilon = 10^{-6}$ and $y = 0$ (upper), $y = -0.1$ (lower).

6 Numerical experiments

In this section we present results of numerical testing of the approaches developed in §§ 3, 4 and 5. We study properties of the approximations of $I(x,y,z)$, with the particular attention to their accuracy and efficacy. Calculations are performed in the numerical computing environment GNU Octave and double precision (64-bit) arithmetics (the machine epsilon ϵ is about $2.22 \cdot 10^{-16}$).

We start presenting computations of the quantity $\mathcal{N}_\varepsilon^{\mathrm{C-C}}(x,y,z)$. Figures 2–4 show in a semi-logarithmic scale the values of $\mathcal{N}_\varepsilon^{\mathrm{C-C}}(x,0,z)$ and $\mathcal{N}_\varepsilon^{\mathrm{C-C}}(x,-0.1,z)$ computed on the grid $(x,z) \in \boldsymbol{L}(800,[-20,0]) \times$

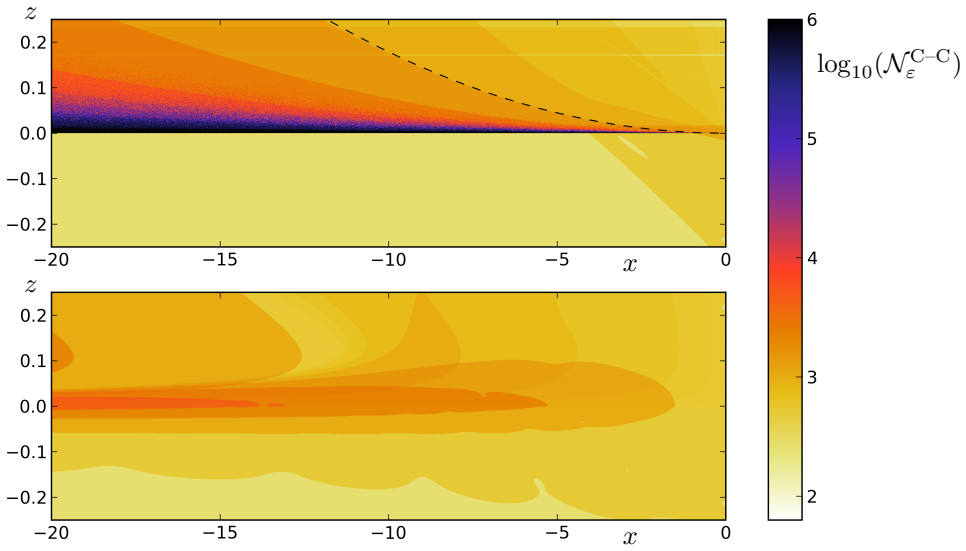

Figure 4: Values of $\log_{10}\bigl(\mathcal{N}_\varepsilon^{\mathrm{C-C}}(x,y,z)\bigr)$ for $\varepsilon = 10^{-12}$ and $y = 0$ (upper), $y = -0.1$ (lower).

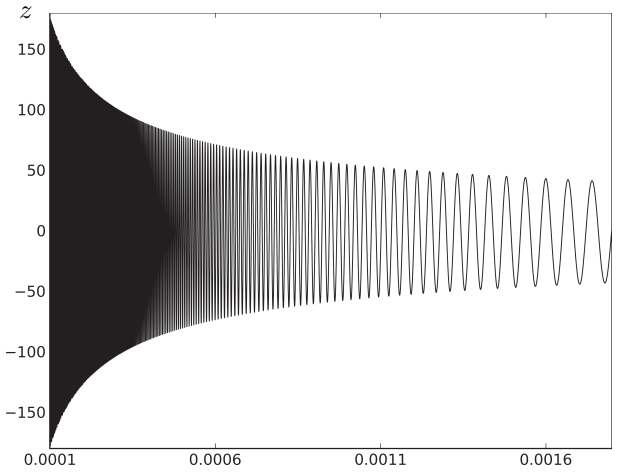

Figure 5: Dependence of $\mathrm{Im}\{I(x,y,z)\}$ on z for fixed $x = -1$, $y = 0$.

$\boldsymbol{L}(800,[-5,5])$ (fig. 2) and $(x,z) \in \boldsymbol{L}(800,[-20,0]) \times \boldsymbol{L}(800,[-0.25,0.25])$ (fig. 3, 4). Here and below $\boldsymbol{L}(n,\gamma)$ is the set consisting of n linearly spaced in the interval γ values (including interval's end-points). The demanded accuracy of computation $\varepsilon = 10^{-6}$ in fig. 2, 3, and $\varepsilon = 10^{-12}$ in fig. 4.

In our computations we set the limit of $2^{19}+1$ evaluations of integrand for each integral in (39), (40). The points, where the accuracy is not achieved with the workload (the inequality (52) is not satisfied), can be easily recognized in the upper part of fig. 4 (the black area located above and close to the x-axis). From the arguments of § 5 (see, in particular, (37)) it is easy to note that the numerical integration of (39), (40) become more difficult with the increase of either of the parameters $D = x^2/(4\sqrt{y^2+z^2})$ or $\theta \in [-\pi/4, \pi/4]$ defined by (38). This happens due to weakening of decay at infinity of the oscillating integrands and naturally leads to accumulation of round-off errors (this effect is more evident for the higher demanded accuracy $\varepsilon = 10^{-12}$). We also note the irregularity of $I(x,y,z)$ for large D: fig. 5 shows the highly oscillating, with

increasing amplitude, behaviour of $\mathrm{Im}\{I(x,0,z)\}$ as $z \to +0$. (Shown in the figure values are computed as $\mathrm{Im}\{I^{\mathrm{C\text{–}C}}_{10^{-6}}(x,y,z)\}$.)

However, we should note that the evaluation of $I^{\mathrm{C\text{–}C}}_{\varepsilon}(x,y,z)$ is reasonably quick and effective up to rather large values of D. For example, the dashed line in fig. 4 corresponds to $D = 100$ (notably, this is the worst case $\theta = \pi/4$ and the accuracy $\varepsilon = 10^{-12}$ is quite close to ϵ). The case of large D has been investigated extensively in [7], where various expansions of $I_\infty(x,y,z;y_0)$ (see (5)) are given and algorithms for numerical evaluation of the function are presented. It is claimed in [7] that the algorithms are applicable and effective for $D > 40$, so they are complementary to our approaches.

Of course, to substantiate the arguments above we should check reliability of the test (52). First, for this purpose we compare $I^{\mathrm{C\text{–}C}}_{\varepsilon_i}(x,y,z)$ for $\varepsilon_1 = 10^{-6}$ and $\varepsilon_2 = 10^{-12}$ to verify that

$$\left|I^{\mathrm{C\text{–}C}}_{\varepsilon_1}(x,y,z) - I^{\mathrm{C\text{–}C}}_{\varepsilon_2}(x,y,z)\right| \le \varepsilon_1. \tag{53}$$

The functions $I^{\mathrm{C\text{–}C}}_{\varepsilon_i}(x,y,z)$ are evaluated for $y = 0$, -0.1, -0.25, -0.5 on the grid $(x,z) \in \boldsymbol{L}(800,[-20,0]) \times \boldsymbol{L}(800,[-0.25,0.25])$. Amidst the checked $2.56 \cdot 10^6$ pairs $I^{\mathrm{C\text{–}C}}_{\varepsilon_1}$, $I^{\mathrm{C\text{–}C}}_{\varepsilon_2}$ (minus 6854 where one or two of the values cannot be computed due to the limit on the number of integrand evaluations) the condition (53) is not satisfied at 8 points (x,z) only. These points correspond to $y = -0.1$, belong to a vicinity of radius 0.05 of $(x,z) = (-15.92, 0.032)$ (so D is quite large, about 603.47) and the maximum found value of the expression in the left-hand side of (53) is approximately equal to $1.85 \cdot 10^{-6}$. Hence, these computations confirm that the criterion of termination (52) is sufficiently reliable.

We can also compare $I^{\mathrm{C\text{–}C}}_{\varepsilon}(x,y,z)$ and the approximation $I^{\mathrm{R5}}_{\varepsilon}(x,y,z)$ introduced in § 4 through an application of the RADAU5 solver [22] to find the solution to (10), (19). It is notable that computation of $I^{\mathrm{R5}}_{\varepsilon}(x,y,z)$ with `ode5r` GNU Octave function is rather stable, failing only for large values of D (e.g. it is possible to compute $I^{\mathrm{R5}}_{\varepsilon}(-1,0,0.008)$ with an accuracy ε better than 10^{-10}). Unfortunately, it is also rather slow, for example, achieving the accuracy $\varepsilon = 10^{-6}$ by $I^{\mathrm{R5}}_{\varepsilon}(-0.1,0,0.01)$ is about 260 slower than the computation of $I^{\mathrm{C\text{–}C}}_{10^{-6}}(-0.1,0,0.01)$. Hence, comparison of $I^{\mathrm{C\text{–}C}}_{\varepsilon}(x,y,z)$ and $I^{\mathrm{R5}}_{\varepsilon}(x,y,z)$ for large sets of (x,y,z) would be too time-consuming. However, to give an example, we evaluate the difference $\left|I^{\mathrm{R5}}_{\varepsilon_1}(x,y,z) - I^{\mathrm{C\text{–}C}}_{\varepsilon_2}(x,y,z)\right|$ for x varying from -10 to 0 with step 0.01 and for fixed $y = 0$, -0.1; $z = 0.1$, 0.2. Since the build-in error estimate in `ode5r` systematically underestimates $|I(x,y,z) - I^{\mathrm{R5}}_{\varepsilon}(x,y,z)|$, we choose $\varepsilon_1 = 10^{-10}$, $\varepsilon_2 = 10^{-6}$ and find the maximal value of the difference $\left|I^{\mathrm{R5}}_{\varepsilon_1}(x,y,z) - I^{\mathrm{C\text{–}C}}_{\varepsilon_2}(x,y,z)\right|$ to be about $1.58 \cdot 10^{-7}$.

Now we compare the two schemes developed in §§ 4, 5 and check the error estimate (36). For these purposes we numerically test the inequality

$$\left|I^{\mathrm{C\text{–}C}}_{\varepsilon}(x,y,z) - \hat{I}^{\mathrm{L\text{–}L}}_{M}(x,y,z)\right| \le \max\left\{\varepsilon^{\mathrm{L\text{–}L}}_{M}(x,y,z), \varepsilon\right\} \tag{54}$$

for $y = 0$, -0.1, -0.25, -0.5, $M = 50$, 100, and $\varepsilon = 10^{-12}$. The functions are evaluated on the grid $(x,z) \in \boldsymbol{L}(400,[-10,0]) \times \boldsymbol{L}(400,[-5,5])$. Amidst the checked $1.28 \cdot 10^6$ pairs $I^{\mathrm{C\text{–}C}}_{\varepsilon}$, $\hat{I}^{\mathrm{L\text{–}L}}_{M}$ corresponding to different values of (x,y,z) and M we found 3145 such that (54) does not hold. All these cases correspond to $y = 0$ and occur near the x-axis, for $z > 0$ and $D > 49$. Besides, all the cases of violation of (54) occur for large values of the error estimate $\varepsilon^{\mathrm{L\text{–}L}}_{M}$ (bigger than 1.15 in our computations). Thus, since we have already got evidence that the test (52) is trustworthy, we can claim that the estimate $\varepsilon^{\mathrm{L\text{–}L}}_{M}$ is fairly adequate and properly overestimates the error $\left|I(x,y,z) - \hat{I}^{\mathrm{L\text{–}L}}_{M}(x,y,z)\right|$ providing the accuracy of approximation is demanded to be sufficiently high (as it is typical in practice).

Fig. 6 shows dependence of $\varepsilon^{\mathrm{L\text{–}L}}_{M}(x,y,z)$ on (x,z) for fixed values $y = 0$, -0.1, -0.25, $M = 50$, 100, in a semi-logarithmic scale. It is interesting to compare the picture with fig. 7 showing

$$\max\left\{-12, \min\left\{0, \log_{10}\left(\left|I^{\mathrm{C\text{–}C}}_{10^{-12}}(x,y,z) - \hat{I}^{\mathrm{L\text{–}L}}_{M}(x,y,z)\right|\right)\right\}\right\}.$$

The values in fig. 6 and 7 are computed on the grid $(x,z) \in \boldsymbol{L}(400,[-10,0]) \times \boldsymbol{L}(400,[-5,5])$. It is important to note that unlike the standard Levin's collocation, our scheme, based on barycentric Lagrange interpolation,

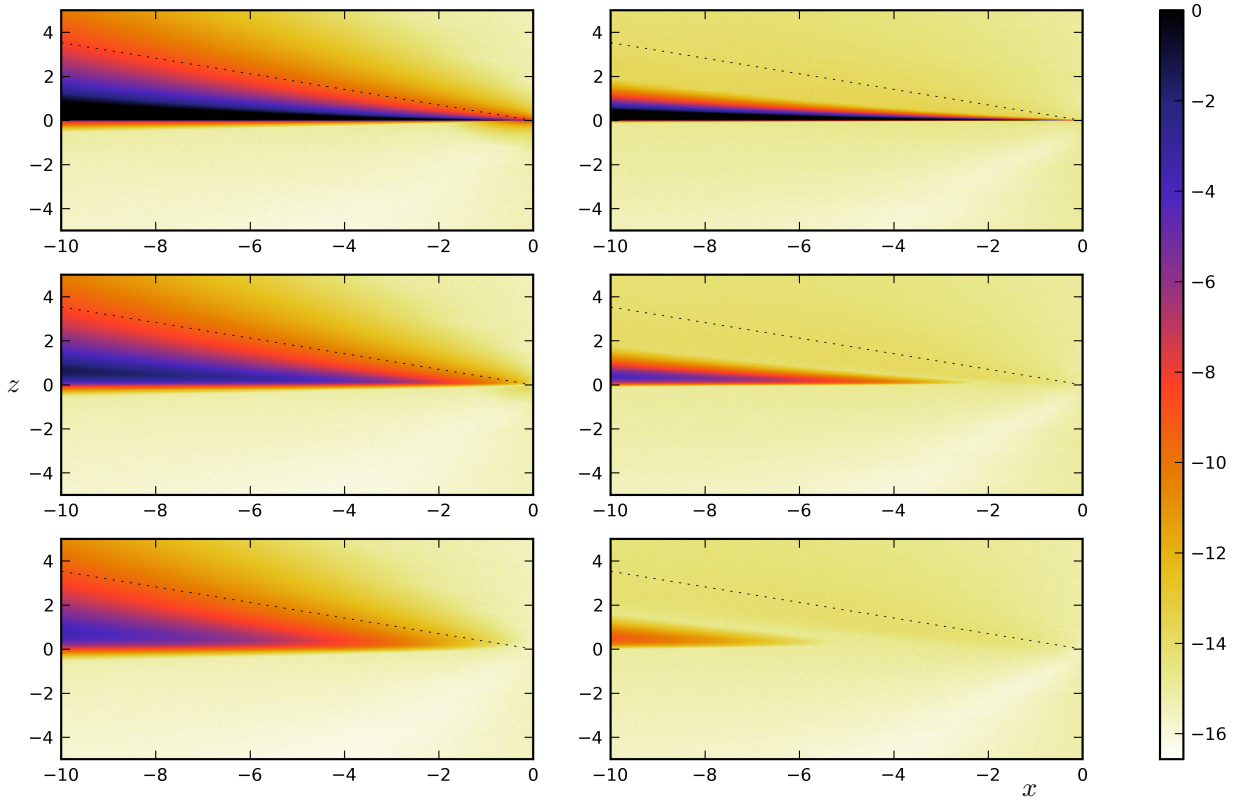

Figure 6: Computation of $\min\left\{0, \log_{10}(\varepsilon_M^{\text{L–L}})\right\}$ as a function of (x, z) for three fixed values $y = 0$, -0.1, -0.25 (from top to bottom) and for $M = 50$ (left column), 100 (right column). The dashed line is locus of equation $x = -2\sqrt{2}z$ (Kelvin angle).

demonstrates numerical stability, its quality increases with growth of M in the representation (27) and it can be applied for M's equal to hundreds and thousands. For example, $\hat{I}_{1000}^{\text{L–L}}(-1, 0, 0.005)$ provides approximation of I with an accuracy better than 10^{-12}. Besides, we have rather satisfactory results for subsets of the domain between the x-axis and the dashed line in fig. 6, 7 — in the presence of critical points of the oscillating integrand in (6). The situation of the presence of critical points is usually avoided in applications of Levin's collocation scheme.

We present some information on the speed of the considered algorithms. To be definitive we state that the computer in use has a 3.4 GHz Intel Core i5 CPU and 8 Gb of RAM. Then, the evaluation time of $\hat{I}_M^{\text{L–L}}(x, y, z)$ is about $1.25 \cdot 10^{-3}$ sec. for $M = 50$, $2.5 \cdot 10^{-3}$ sec. for $M = 100$, $9 \cdot 10^{-3}$ sec. for $M = 200$. Time of evaluation of $I_\varepsilon^{\text{C–C}}(x, y, z)$ depends on the number of integrands evaluations in (39), (40), needed to achieve the accuracy ε; the time is about 10^{-2} when $\log_{10} \mathcal{N}_\varepsilon^{\text{C–C}} \approx 4.2$ and about $2.5 \cdot 10^{-3}$ when $\log_{10} \mathcal{N}_\varepsilon^{\text{C–C}} \approx 2.4$ (see Figures 2–4).

The experience of computations shows that the procedures $\hat{I}_M^{\text{L–L}}(x, y, z)$ and $I_\varepsilon^{\text{C–C}}(x, y, z)$ spend comparable time to provide an approximation of $I(x, y, z)$ with the given accuracy ε. It can be observed that the algorithm based on Levin's ODE and barycentric Lagrange interpolation is considerably faster than the counterpart when the value of M, needed to achieve the given accuracy, is small. The situation of small M is, in particular, typical for large $|y|$; for instance, we need $M = 20$ for $x = -1$, $y = -1$, $z = 0.1$, $\varepsilon = 10^{-12}$ and $\hat{I}_M^{\text{L–L}}(x, y, z)$ is more than 3 times faster. However, unlike the algorithm based on Clenshaw–Curtis quadrature — designed to provide the result with the demanded accuracy — in the algorithm based on Levin's

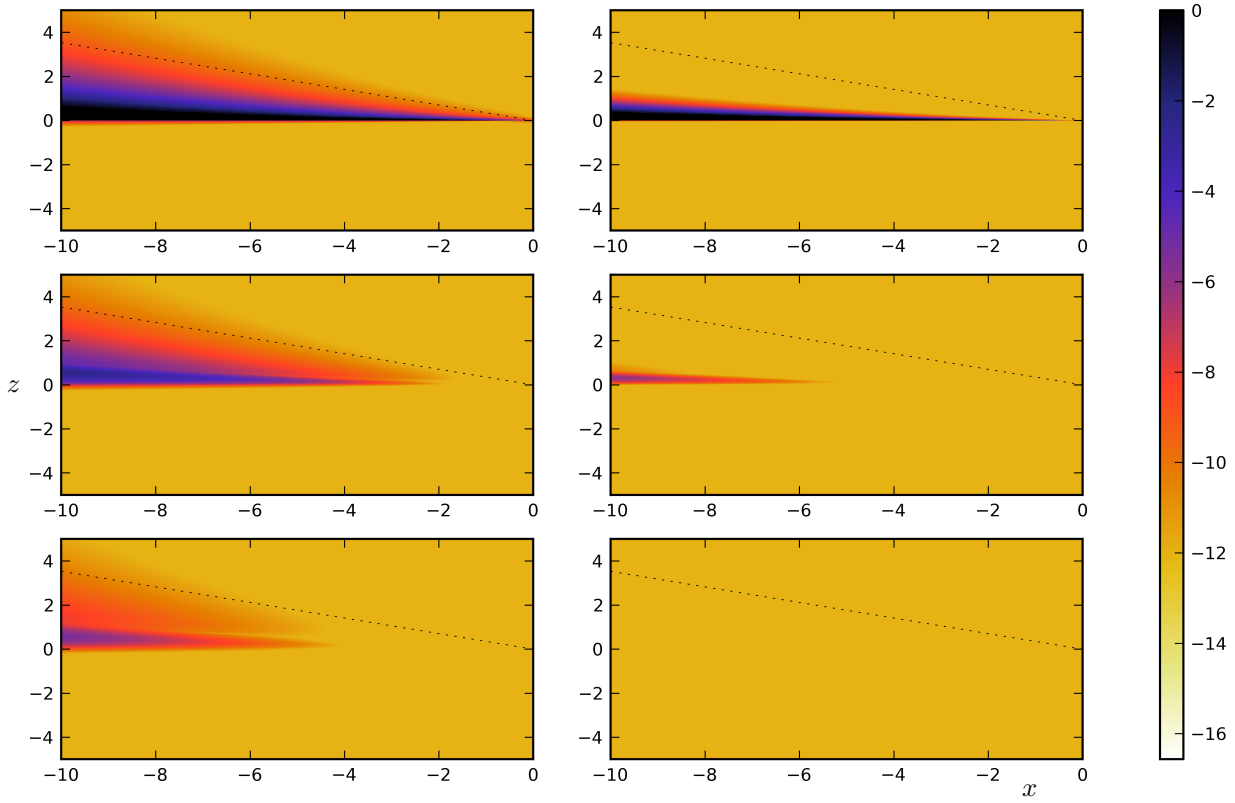

Figure 7: Computation of $\max\Big\{-12, \min\Big\{0, \log_{10}\Big(\big|I^{\text{C–C}}_{10^{-12}}(x,y,z) - \hat{I}^{\text{L–L}}_{M}(x,y,z)\big|\Big)\Big\}\Big\}$ as a function of (x,z) for three fixed values $y = 0,\ -0.1,\ -0.25$ (from top to bottom) and for $M = 50$ (left column), 100 (right column). The dashed line is locus of equation $x = -2\sqrt{2}z$ (Kelvin angle).

ODE and Lagrange interpolation the number M guaranteeing the accuracy ε is not known a-priori. However, fig. 6 and 7 show that the approximation error by $\hat{I}^{\text{L–L}}_{M}(x,y,z)$ is quite regular and predictable. Consider a fixed ε and test $I^{\text{L–L}}_{M}(x,y,z)$ against $I^{\text{C–C}}_{\varepsilon/2}(x,y,z)$ for a grid of (x,y,z). For each point (x,y,z) of the grid we find minimal $M_\varepsilon(x,y,z)$ guaranteeing that $\big|I^{\text{C–C}}_{\varepsilon/2}(x,y,z) - \hat{I}^{\text{L–L}}_{M}(x,y,z)\big| \le \varepsilon/2$. (This should be a rather trivial but time-consuming operation.) Suppose that a simple majorizing function $\mathcal{M}_\varepsilon(x,y,z) \ge M_\varepsilon(x,y,z)$ is proposed, then we could use $\hat{I}^{\text{L–L}}_{\mathcal{M}_\varepsilon(x,y,z)}(x,y,z)$ to provide the result with the given accuracy ε. However, such study is beyond of our scope in the present paper.

Along with the convenience to provide the approximation of $I(x,y,z)$ with the given accuracy, another advantage of the algorithm based on the Clenshaw–Curtis quadrature is its ability to work rather well (naturally, becoming slower) for large D and θ close to $\pi/4$. As fig. 3, 4 show, for reasonable accuracy, say, $\varepsilon = 10^{-6}$–10^{-7} — not allowing the limitations of the double-float arithmetics to manifest themselves — the values of D can be very large (on the standards of [7]). To give an example, we stay within the limit of $2^{19}+1$ evaluations of each integrand in (40) when computing $I^{\text{C–C}}_{10^{-7}}\big(x, 0, 10^{-6}\big)$ for x varying from -1 to 0 with the step 10^{-5}. (Note that $D(-1, 0, 10^{-6})$ is as large as $2.5 \cdot 10^5$.)

Finally, we can conclude that both procedures $I^{\text{C–C}}_{\varepsilon}(x,y,z)$ and $\hat{I}^{\text{L–L}}_{M}(x,y,z)$ are sufficiently fast and reliable. These algorithms are complementary to those of [7], developed for large D. The algorithm based on Clenshaw–Curtis quadrature is rather universal, provides results with the given accuracy and is applicable for very large values of D. The algorithm based on Levin's ODE and the barycentric Lagrange interpolation has advantages when the number M needed for achieving a given accuracy ε is sufficiently small.

z \ y	-0.5	-0.1	-0.01	0
0.5	-0.3132089735	-0.4347821474	-0.4093149760	-0.4039184710
0.1	-0.4288349681	-1.0716691716	-2.1157417380	-2.5160949098
0.01	-0.4349760923	-0.9188289512	-0.7896492217	3.6856412628

Table 1: Benchmark values of $I_\infty(x,y,z)$ defined by (5) for $x=-1$ and a variety of (y,z).

7 Computation of derivatives of $I(x,y,z)$

In this section we consider application of the suggested methods to computation of derivatives of $I(x,y,z)$ and show that the generalization is rather straightforward. Let us introduce a vector $\boldsymbol{\ell}=(\ell_1,\ell_2,\ell_3)^{\mathsf{T}}$ and consider

$$J(\boldsymbol{\ell},\boldsymbol{x}) := \nabla I(x,y,z)\cdot\boldsymbol{\ell} = \int_0^\infty \varpi(t,\ell_1,\ell_2,\ell_3)\mathrm{e}^{\varpi(t,x,y,z)}\,\mathrm{d}t, \tag{55}$$

where the function ϖ is defined by (6).

First, we note that in view of smoothness and polynomial behaviour at infinity of the function $\varpi(t,\boldsymbol{\ell})$ the scheme of § 5 can be used for evaluation of $J(\boldsymbol{\ell},\boldsymbol{x})$ without any amendments or restrictions.

Consider now application of the scheme developed in § 3, 4 to computation of (55). Similarly to (7) we write

$$J(\boldsymbol{\ell},\boldsymbol{x}) = \int_0^1 \varpi_*(\tau,\boldsymbol{\ell})\frac{\mathrm{e}^{\varpi_*(\tau,\boldsymbol{x})}}{(1-\tau)^2}\,\mathrm{d}t,$$

where again $\varpi_*(\tau,\boldsymbol{x})=\varpi(\tau/(1-\tau),\boldsymbol{x})$. Then we use (8) and find that

$$J(\boldsymbol{\ell},\boldsymbol{x}) = \frac{\Psi_{\boldsymbol{\ell},\boldsymbol{x}}(\tau)}{(1-\tau)^2}\mathrm{e}^{\varpi_*(\tau,\boldsymbol{x})}\Big|_{\tau=0}^{\tau=1}, \tag{56}$$

if for the given $\boldsymbol{\ell}$ and $\boldsymbol{x}$ the function $\Psi_{\boldsymbol{\ell},\boldsymbol{x}}(\tau)$ satisfies the equation

$$\Psi'_{\boldsymbol{\ell},\boldsymbol{x}}(\tau) + \frac{2\,\Psi_{\boldsymbol{\ell},\boldsymbol{x}}(\tau)}{1-\tau} + \partial_\tau\varpi_*(\tau,\boldsymbol{x})\,\Psi_{\boldsymbol{\ell},\boldsymbol{x}}(\tau) = \varpi_*(\tau,\boldsymbol{\ell}).$$

Since $\varpi_*(\tau,\boldsymbol{\ell})=O((1-\tau)^{-2})$ as $\tau\to1$, it is convenient to define $\Psi_{\boldsymbol{\ell},\boldsymbol{x}}(\tau)=(1-\tau)\,\Phi_{\boldsymbol{\ell},\boldsymbol{x}}(\tau)$. Then, $\Phi_{\boldsymbol{\ell},\boldsymbol{x}}(\tau)$ satisfies the following differential equation

$$(1-\tau)^3\,\Phi'_{\boldsymbol{\ell},\boldsymbol{x}}(\tau) + \big[(1-\tau)^2+\sigma(\tau,\boldsymbol{x})\big]\,\Phi_{\boldsymbol{\ell},\boldsymbol{x}}(\tau) = \varpi_\circ(\tau,\boldsymbol{\ell}), \tag{57}$$

where σ is defined by (9) and $\varpi_\circ(\tau,\boldsymbol{\ell})=(1-\tau)^2\,\varpi_*(\tau,\boldsymbol{\ell})$.

Analogously to (12), (14), assuming $y<0$ we can find the bounded on $[0,1]$ solution of (57)

$$\Phi_{\boldsymbol{\ell},\boldsymbol{x}}(\tau) = (\tau-1)\mathrm{e}^{\Lambda(\tau,\boldsymbol{x})}\int_\tau^1 \frac{\varpi_\circ(\tau,\boldsymbol{\ell})\mathrm{e}^{-\Lambda(\theta,\boldsymbol{x})}}{(\theta-1)^4}\,\mathrm{d}\theta,$$

where $\Lambda(\tau,\boldsymbol{x})$ is defined by (13). We write

$$\Phi_{\boldsymbol{\ell},\boldsymbol{x}}(\tau) = (\tau-1)\mathrm{e}^{\Lambda(\tau,\boldsymbol{x})}\int_\tau^1 \frac{\mathrm{e}^{-\frac{\gamma_2}{(\theta-1)^2}-\frac{\gamma_1}{\theta-1}-\gamma_0}}{(\theta-1)^4}\,[c_0^*(\boldsymbol{\ell})+\varrho(\theta,\boldsymbol{\ell},\boldsymbol{x})]\,\mathrm{d}\theta,$$

where $c_0^*(\boldsymbol{\ell})=\varpi_\circ(1,\boldsymbol{\ell})=\ell_2+\mathrm{i}\ell_3$ and for $\theta\in[0,1]$, $|\varrho(\theta,\boldsymbol{\ell},\boldsymbol{x})|\le C^*(\boldsymbol{\ell},\boldsymbol{x})|\theta-1|$, $C^*(\boldsymbol{\ell},\boldsymbol{x})$ is constant in θ. Thus, we find

$$\Phi_{\boldsymbol{\ell},\boldsymbol{x}}(\tau) = (\tau-1)\mathrm{e}^{\Lambda(\tau,\boldsymbol{x})}\left\{c_0^*(\boldsymbol{\ell})\,L_0^*(\tau,\boldsymbol{x})+\check{L}(\tau,\boldsymbol{\ell},\boldsymbol{x})\right\},\quad\text{where} \tag{58}$$

$$L_0^*(\tau,\boldsymbol{x}) = \int_\tau^1 (\theta-1)^{-4}\mathrm{e}^{-\frac{\gamma_2}{(\theta-1)^2}-\frac{\gamma_1}{\theta-1}-\gamma_0}\,\mathrm{d}\theta,\quad \check{L}(\tau,\boldsymbol{\ell},\boldsymbol{x}) = \int_\tau^1 \frac{\varrho(\theta,\boldsymbol{\ell},\boldsymbol{x})}{(\theta-1)^4}\mathrm{e}^{-\frac{\gamma_2}{(\theta-1)^2}-\frac{\gamma_1}{\theta-1}-\gamma_0}\,\mathrm{d}\theta.$$

Further we obtain (cf. (17))

$$L_0^*(\tau,\boldsymbol{x}) = \frac{\sqrt{\pi}}{8\gamma_2^{5/2}}(\gamma_1^2+2\gamma_2)\mathrm{e}^{-\gamma_0+\frac{\gamma_1^2}{4\gamma_2}}\operatorname{erfc}\left(\frac{\sqrt{\gamma_2}}{1-\tau}-\frac{\gamma_1}{2\sqrt{\gamma_2}}\right)+\frac{1}{4\gamma_2^2}\mathrm{e}^{-\frac{\gamma_2}{(\tau-1)^2}-\frac{\gamma_1}{\tau-1}-\gamma_0}\left(\gamma_1+\frac{2\gamma_2}{1-\tau}\right). \quad (59)$$

Define the function

$$\lambda(\tau,y) = \frac{\sqrt{\pi}}{4|y|^{3/2}}(1+2|y|)\mathrm{e}^{|y|}\operatorname{erfc}\left(\frac{\sqrt{|y|}\tau}{1-\tau}\right)+\frac{1}{2|y|}\mathrm{e}^{\frac{y}{(\tau-1)^2}+\frac{2y}{\tau-1}}\left(1+\frac{1}{1-\tau}\right) \quad (60)$$

(the expression is obtained by replacing γ_0, γ_1, γ_2 by by their real parts in the right-hand side of (59)). Then, for $\tau \le 1$ we find $|\check{L}(\tau,\boldsymbol{\ell},\boldsymbol{x})| \le C^*(\boldsymbol{\ell},\boldsymbol{x})(1-\tau)\lambda(\tau,y)$ and, thus, in view of (60) and [1, 7.1.23], we have as $\tau \to 1-0$:

$$\left|(\tau-1)\mathrm{e}^{\Lambda(\tau,\boldsymbol{x})}\,\check{L}(\tau,\boldsymbol{\ell},\boldsymbol{x})\right| = O(\tau-1). \quad (61)$$

Using (58), (59), (61), and [1, 7.1.23] we obtain the representation

$$\Phi_{\boldsymbol{\ell},\boldsymbol{x}}(\tau) = \Phi_{\boldsymbol{\ell},\boldsymbol{x}}(1) + O(\tau-1), \quad \text{where}$$
$$\Phi_{\boldsymbol{\ell},\boldsymbol{x}}(1) := \lim_{\tau\to 1-0}\Phi_{\boldsymbol{\ell},\boldsymbol{x}}(\tau) = \frac{\ell_2+\mathrm{i}\ell_3}{2(y+\mathrm{i}z)}. \quad (62)$$

Finally, for $y<0$ by (56) we have $J(\boldsymbol{\ell},\boldsymbol{x}) = -\Phi_{\boldsymbol{\ell},\boldsymbol{x}}(0)\mathrm{e}^{y+\mathrm{i}x}$. The numerical solution to (57), (62) can be sought using the scheme described in § 4. When we seek the approximation of $\Phi_{\boldsymbol{\ell},\boldsymbol{x}}(\tau)$ in the form (27) we can define the first term of the expansion as follows:

$$\hat{\phi}_{\boldsymbol{\ell},\boldsymbol{x}}(\tau) = c_0^*(\boldsymbol{\ell})(\tau-1)\mathrm{e}^{\frac{\gamma_2}{(\tau-1)^2}+\frac{\gamma_1}{\tau-1}+\gamma_0}\,L_0^*(\tau,\boldsymbol{x})$$

(see (58)). It is also straightforward to compute $\mathcal{L}\hat{\phi}_{\boldsymbol{\ell},\boldsymbol{x}}(\tau)$ analogously to (30).

8 Conclusion

In this paper we deal with the problem of evaluation of the Green's function for the classical linear ship-wave problem describing forward motion of bodies in unbounded heavy fluid having a free surface. Of interest for us is the wavelike (often referred to as 'single integral') term $I_\infty(x,y,z)$ which represents the dominating in the far-field, oscillatory part of Green's function. The integral $I_\infty(x,y,z)$ is expressed (5) in terms of the integral $I(x,y,z)$. Our purpose is to elaborate accurate and fast computation techniques to approximate $I(x,y,z)$ and its derivatives. At that, the main difficulty is due to the presence in the integrand of two oscillating factors of different nature and the infinite interval of integration. The oscillating integrand can have stationary points and there is a difficult limiting case — the track of the source moving in the free surface is a line of essential singularities of the considered integral.

First, by using the ideas of Levin [33, 34] we reduce evaluation of the integral to solution of an ordinary differential equation on the interval $[0,1]$. We prove that the equation has one bounded solution, whose value at the right end of the interval is known, while the value at the left end, up to a known factor, coincides with the sought value of $I(x,y,z)$. To find the solution of the differential equation numerically we develop an algorithm based on usage of Lagrange interpolating polynomial in a barycentric form and collocation of the equation on a set of Chebyshev points. Another representation of the solution to the differential equation consists of the polynomial and a term arising from an asymptotic analysis. An estimate for the residual of solution is suggested and numerically tested to demonstrate its reliability. It is notable that, unlike the standard Levin's collocation based on expansion in Chebyshev polynomials, the suggested scheme demonstrates numerical stability.

Secondly, we develop an alternative numerical algorithm based on the Clenshaw–Curtis quadrature [8] and involving transformation of the integral path using the steepest descent method. The advantages of the quadrature rule are its fast convergence, simple and effective computation of weights (even for very large number of nodes), excellent numerical stability. Relying upon the properties and taking into account the simplicity of the integrand, we suggest to apply the quadrature in 'brute force' manner, increasing the number of its nodes (doubled at each step) until some last values of the sequence of approximations become closer to each other with the given tolerance.

These two alternative methods are tested numerically and compared for a wide variety of parameters, with special attention to the accuracy and efficacy. The experiments show that both algorithms are reliable, compatible in speed and much faster than standard solvers being applied to the Levin's differential equation. The algorithm based on Levin's equation and barycentric Lagrange interpolation is somewhat faster when the order of interpolating polynomial, needed for achieving the given accuracy, is small. At the same time, the algorithm based on the Clenshaw–Curtis quadrature is more convenient to evaluate $I(x, y, z)$ to the given accuracy and the algorithm works better in the most difficult for the numerical integration zone near the track of the source moving close to the free surface.

Finally, in the present work we discuss application of the suggested methods to computation of derivatives of $I(x, y, z)$ and show that their generalization is rather straightforward.

References

[1] M. Abramowitz, I. A. Stegun (Eds.) *Handbook of Mathematical Functions*, Dover, New York, 1965.

[2] J. J. M. Baar, W. G. Price, Evaluation of the wavelike disturbance in the Kelvin wave source potential, *J. Ship Research* **32** (1988) 44–53.

[3] J. J. M. Baar, W. G. Price, Developments in the calculation of the wavemaking resistance of ships, *Proc. R. Soc. London A* **416**(1850) (1988) 115–147.

[4] J.-P. Berrut, L.N. Trefethen, Barycentric Lagrange interpolation, *SIAM Rev.*, **46** (2004) 501–517.

[5] M. Bessho, On the fundamental function in the theory of the wave-making resistance of ships, *Memoirs of the Defense Academy of Japan*, **4**(2) (1964) 99–119.

[6] X. Chen, Role of the surface tension in modelling ship waves, In: R.C. Rayney, S.F. Lee (Eds.), *Proc. of the 17th Inter. Workshop on water Waves and floating bodies*, Peterhouse Cambridge, UK, 2002, pp. 25–28.

[7] J.-M. Clarisse, J.N. Newman, Evaluation of the wave-resistance Green function: Part 3 – The single integral near the singular axis, *J. Ship Research.* **38**(1) (1994) 1–8.

[8] C.W. Clenshaw, A.R. Curtis, A method for numerical integration on an automatic computer, *Numerische Mathematik* **2** (1960) 197–205.

[9] A. Darmon, M. Benzaquen, E. Raphaël, Kelvin wake pattern at large Froude numbers, *Journal of Fluid Mechanics* **738** (2014), R3 (8 pages), doi:10.1017/jfm.2013.607.

[10] A. Deaño, D. Huybrechs, Complex Gaussian quadrature of oscillatory integrals, *Numerische Mathematik* **112** (2009) 197–219.

[11] V. Domínguez, I.G. Graham, T. Kim, Filon–Clenshaw–Curtis rules for highly oscillatory integrals with algebraic singularities and stationary points, *SIAM J. Numerical Analysis* **51**(3) (2013) 1542–1566.

[12] K. Eggers, On far-field approximations to the wave pattern around a ship travelling at constant velocity. In: P.A. Martin, G.R. Wickham (Eds.), *Wave Asymptotics*, Cambridge University Press, New York, 1992, pp. 136–159.

[13] D. Euvrard, *Les mille et une facéties de la fonction de Green du problème de la résistance de vagues*, Rapport de Recherche no. 144, Ecole Nationale Supérieure de Techniques Avancées, France, 1983.

[14] G.A. Evans, K.C. Chung, Some theoretical aspects of generalised quadrature methods, *J. Complexity* **19** (2003) 272–285.

[15] G.A. Evans, J.R. Webster, A comparison of some methods for the evaluation of highly oscillatory integrals, *Journal of Computational and Applied Mathematics*, **112** (1999) 55–69.

[16] V.N. Faddeyeva, N.M. Terent'ev, *Tables of the probability integral for complex argument*. Pergamon Press, Oxford, 1961.

[17] L.N.G. Filon, On a quadrature formula for trigonometric integrals, *Proc. Roy. Soc. Edinburgh* **49** (1928) 38–47.

[18] E.A. Flinn, A modification of Filon's method of numerical integration, *Journal of the ACM* **7**(2) (1960) 181–184.

[19] A. Gamst, *Existenz, Eindeutigkeit und Regularitat stationarer Wellen Stromungen, die von Druck Verteilungen an der Wasseroberflache verursacht werden. Lineare Theorie*, Univ. Hamburg. Ph.D. Thesis, 1979.

[20] W.M. Gentleman, Implementing Clenshaw–Curtis quadrature, I, Methodology and experience, *Communications of the ACM* **15** (1972) 337–342.

[21] W.M. Gentleman, Implementing Clenshaw–Curtis Quadrature, II, Computing the Cosine Transformation, *Communications of the ACM* **15** (1972) 343–346.

[22] E. Hairer, G. Wanner, *Solving ordinary differential equations II: Stiff and differential-algebraic problems*, 2nd revised edition, Springer-Verlag, 1996.

[23] P. Henrici, Barycentric formulas for interpolating trigonometric polynomials and their conjugates, *Numerische Mathematik*, **33** (1979) 225–234.

[24] N.J. Higham, The numerical stability of barycentric Lagrange interpolation, *IMA Journal of Numerical Analysis* **24** (2004) 547–556.

[25] D. Huybrechs, S. Olver, Highly oscillatory quadrature. In: B. Engquist, A. Fokas, E. Hairer, A. Iserles (Eds.), *Highly Oscillatory Problems*, Cambridge Univ. Press, Cambridge, 2009, pp. 25–50.

[26] D. Huybrechs, S. Vandewalle, On the evaluation of highly oscillatory integrals by analytic continuation, *SIAM J. Numer. Anal.* **44** (2007) 1026–1048.

[27] A. Iserles, S.P. Nørsett, Efficient quadrature of highly oscillatory integrals using derivatives, *Proc. R. Soc. London A* **461** (2005) 1383–1399.

[28] A. Iserles, S.P. Nørsett, S. Olver, Highly oscillatory quadrature: the story so far. *Numerical Mathematics and Advanced Applications* (2006) 97–118.

[29] S.G. Johnson, *Faddeeva Package, free/open-source C++ implementation*, MIT, 2012, online: http://ab-initio.mit.edu/wiki/index.php/Faddeeva Package.

[30] T. Kaneko, B. Liu, Accumulation of round-off error in fast Fourier transforms, *Journal of the ACM* **17** (1970) 637–654.

[31] N. Kuznetsov, V. Maz'ya, B. Vainberg, *Linear water waves: a Mathematical Approach*. Cambridge University Press, Cambridge, 2002.

[32] L. Larsson, E. Baba, Ship resistance and flow computations. In: M. Ohkusu (Ed.), *Advances in Marine Hydrodynamics*, Computational Mechanics Publications, Southampton, Boston, 1996, pp. 1–75.

[33] D. Levin, Procedures for computing one and two-dimensional integrals of functions with rapid irregular oscillations, *Mathematics of Computation* **38**(158) (1982) 531–538.

[34] D. Levin, Analysis of a collocation method for integrating rapidly oscillatory functions, *Journal of Computational and Applied Mathematics* **78** (1997) 131–138.

[35] J. Li, X. Wang, T. Wang, A universal solution to one-dimensional oscillatory integrals, *Science in China Series F: Information Sciences* **51** (2008) 1614–1622.

[36] J. Li, X. Wang, T. Wang, S. Xiao, An improved Levin quadrature method for highly oscillatory integrals. *Applied Numerical Mathematics* **60** (2010) 833–842.

[37] J. Li, X. Wang, T. Wang, S. Xiao, M. Zhu, On an improved-Levin oscillatory quadrature method, *Journal of Mathematical Analysis and Applications* **380**(2) (2011) 467–474.

[38] G. Marr, *An investigation of Neumann–Kelvin ship wave theory and its application to yacht*, PhD thesis, University of Auckland, New Zealand, 1995.

[39] V. G. Maz'ya, B. R. Vainberg, On ship waves, *Wave Motion* **18** (1993) 31–50.

[40] T. Miloh, *Mathematical approaches in hydrodynamics*, SIAM, Philadelphia, 1991.

[41] O.V. Motygin, On well-posed statements of the three-dimensional ship-wave problem, *Quarterly Journal of Mechanics and Applied Mathematics* **65**(3) (2012) 389–408.

[42] J.N. Newman, Evaluation of the wave-resistance Green function. Part 1. The double integral, *J. Ship Research* **31** (1987) 79–90.

[43] F. Noblesse, The fundamental solution in the theory of steady motion of a ship, *J. Ship Research* **21** (1977) 82–88.

[44] F. Noblesse, Alternative integral representations for the Green function of the theory of ship wave resistance, *Journal of Engineering Mathematics* **15**(4) (1981) 241–265.

[45] H. O'Hara, F.J. Smith, Error estimation in the Clenshaw–Curtis quadrature formula, *The Computer Journal* **11**(2) (1968) 213–219.

[46] S. Olver, Moment-free numerical approximation of highly oscillatory integrals with stationary points, *European Journal of Applied Mathematics* **18**(4) (2007) 435–447.

[47] S. Olver, *Numerical approximation of highly oscillatory integrals*, PhD thesis, University of Cambridge, UK, 2008.

[48] S. Olver, Fast, numerically stable computation of oscillatory integrals with stationary points, *BIT Numerical Mathematics* **50**(1) (2010) 149–171.

[49] T. Ooura, A double exponential formula for the Fourier transforms, *Publications of the Research Institute for Mathematical Sciences, Kyoto University* **41** (2005) 971–978.

[50] B. Ponizy, M. Guilbaud, M. Ba, Numerical computations and integrations of the wave resistance Greens function, *Theoretical and Computational Fluid Dynamics* **12** (1998) 179–194.

[51] M. Rabaud, F. Moisy, Ship wakes: Kelvin or Mach angle ? *Phys. Rev. Lett.* **110** (2013) 214503.

[52] A.M. Reed, J.H. Milgram, Ship wakes and their radar images, *Annual Review of Fluid Mechanics* **34** (2002) 469–502.

[53] H.E. Salzer, Lagrangian interpolation at the Chebyshev Points $x_{n,\nu} \equiv \cos(\nu\pi/n)$, $\nu = 0(1)n$; some unnoted advantages, *The Computer Journal* **15**(2) (1972) 156–159.

[54] H.T. Shen, C. Farell, Numerical calculation of the wave integrals in the linearized theory of water waves, *J. Ship Research* **21** (1977) 1–10.

[55] W. Thomson (Lord Kelvin), On ship waves, *Proc. Inst. Mech. Eng.* (1887) 409–433; also *Popular lectures and addresses* **II** (1891) 450–500.

[56] L.N. Trefethen, Is Gauss quadrature better than Clenshaw–Curtis? *SIAM Review* **50** (2008) 67–87.

[57] L.N. Trefethen, *Approximation theory and approximation in practice*, SIAM, 2013.

[58] F. Ursell, On Kelvin's ship wave pattern, *J. Fluid Mechanics* **8** (1960) 418–431.

[59] F. Ursell, On the theory of the Kelvin ship-wave source: asymptotic expansion of an integral, *Proc. Roy. Soc. London A* **418** (1988) 81–93.

[60] J. Waldvogel, Fast construction of the Fejér and Clenshaw–Curtis quadrature rules, *BIT Numerical Mathematics* **46** (2006) 195–202.

[61] H.T. Wang, J.C. Rogers, Numerical evaluation of the complete wave-resistance Green function using Bessho's approach, In: K. Mori (Ed.), *5th International Conference on Numerical Ship Hydrodynamics*, The National Academies Press, Washington, D.C., 1990, pp. 133–144.

[62] J.V. Wehausen, The wave resistance of ships, *Advances in Applied Mechanics* **13** (1973) 93–245.

[63] J.V. Wehausen, E.V. Laitone, *Surface waves*, In: S. Flügge (Ed.), C. Truesdell (Co-ed.), Encyclopaedia of Physics, Volume IX, Fluid dynamics III, Springer-Verlag, Berlin, 1960, pp. 446–778. Online: http://www.coe.berkeley.edu/SurfaceWaves/

[64] S. Xiang, On the Filon and Levin methods for highly oscillatory integral $\int_a^b f(x)\mathrm{e}^{\mathrm{i}\omega\, g(x)}\mathrm{d}x$, *J. Computational and Applied Mathematics* **208** (2007) 434–439.